2020-03

Theoretical and experimental studies of imidazolium based ionic liquids for supercapacitors application

Chengula, Plassidius Joachim

THEORETICAL AND EXPERIMENTAL STUDIES OF IMIDAZOLIUM-BASED IONIC LIQUIDS FOR SUPERCAPACITORS APPLICATION

Plassidius Joachim Chengula

A Dissertation Submitted in Partial Fulfillment of the Requirements for the Degree of Master's in Materials Science and Engineering of the Nelson Mandela African Institution of Science and Technology

Arusha, Tanzania

March, 2020

ABSTRACT

The theoretical study of neutral ion pairs of 1-ethyl-3-methylimidazolium tetrafluoroborate ([EMIM][BF4]) and 1-ethyl-3-methylimidazolium bis(trifluoromethylsulfonyl)imide ([EMIM][NTf_2]) has been performed. The formation of the neutral ion pairs was considered through interionic reactions involving the $[EMIM]^+$ cation and two anions, $[BF_4]^-$ and $[NTf_2]^-$. Computations were performed by the DFT/6-311++G(d,p) method with B3LYP5 and CAM–B3LYP functionals. The enthalpies of the interionic reactions $\Delta_r H°(0)$ have been determined theoretically for both ion pairs. In addition, following the available experimental data for [EMIM][NTf_2], the enthalpy of the reaction based on experiment was obtained. The recommended values of $\Delta_r H°(0)$ are as follows: –359 ± 15 kJ mol^{-1} for [EMIM][BF_4] and –323 ± 9 kJ mol^{-1} for [EMIM][NTf_2]. The thermodynamic stability of the ion pairs was interpreted through analysis of the frontier molecular orbitals as well as simple ionic model. Experimental test on influence of imidazolium-based ionic liquids in electrochemical system was investigated, with the potential window of 2.8 V for both ionic liquids. The specific capacitances were found to be 4.1 F g^{-1} and 4.3 F g^{-1} for [EMIM][BF_4] and [EMIM][NTf_2] respectively, at the lower scan rate of 5 mV s^{-1}. The maximum current densities reached were 87 mA g^{-1} and 88 mA g^{-1} for [EMIM][BF_4] and [EMIM][NTf_2], respectively. Electrochemical measurements by cyclic voltammetry and electrochemical impedance spectroscopy have been conducted on three electrodes system with the IILs under study. A supercapacitor prototype has been fabricated; conventional charge-discharge tests were done.

Keywords: Ionic liquids, density functional theory, thermodynamic functions, supercapacitor, cyclic voltammetry, electrochemical impedance spectroscopy

DECLARATION

I, Plassidius Joachim Chengula do hereby declare to the Senate of The Nelson Mandela African Institution of Science and Technology that this dissertation is my original work and that it has neither been submitted nor being concurrently submitted for degree award in any other institution.

Plassidius Joachim Chengula

Name and Signature of candidate	**Date**

The above declaration is confirmed by

Prof. Alexander M. Pogrebnoi

Name and Signature of supervisor 1	**Date**

Prof. Tatiana Pogrebnaya

Name and Signature of supervisor 2	**Date**

COPYRIGHT

CERTIFICATION

The undersigned certify that they have read and hereby recommend for examination by The Nelson Mandela African Institution of Science and Technology a dissertation/thesis entitled: Theoretical and Experimental Studies of Imidazolium based Ionic Liquids for Supercapacitors Application, in (partial) fulfillment of the requirements for the degree of Master's in Materials Science and Engineering of The Nelson Mandela African Institution of Science and Technology.

Prof. Alexander M. Pogrebnoi

Name and Signature of supervisor 1	**Date**

Prof. Tatiana Pogrebnaya

Name and Signature of supervisor 2	**Date**

ACKNOWLEDGEMENTS

I wish to express my appreciation to my supervisors Prof. Alexander Pogrebnoi, as well as Prof. Tatiana Pogrebnaya, for their unlimited support. My special thanks are expressed to my course instructors Prof. Alexander Pogrebnoi, Prof. Tatiana Pogrebnaya, Dr. Askwar Hilonga and others who laid the fundamentals of my research, though it was hard, they never gave up taking this heavy weighted burden. Also, I wish to extend my sincere thanks to my academic staffs and my classmates in the Department of Materials, Energy Science and Engineering. May the Almighty God, always look at you with eyes of love.

I extend my earnest appreciations to Mkwawa University College of Education, A Constituent College of the University of Dar es Salaam for granting me a study leave without forgetting the Centre of Excellence named Water Infrastructure and Sustainable Energy Futures (WISE-Future) for sponsoring my studies. The Nelson Mandela Institution of Science and Technology (NM-AIST) is also acknowledged for offering me a room to utilize whatever resource available throughout my studies.

DEDICATION

This work is dedicated to my:

Family

Friends

TABLE OF CONTENTS

LIST OF TABLES

LIST OF FIGURES

LIST OF APPENDICES

LIST OF ABBREVIATIONS AND SYMBOLS

$[BF_4]^-$	Tetrafluoroborate anion
[EMIM][BF_4]	1-Ethyl-3-methylimidazolium tetrafluoroborate
[EMIM][NTf_2]	1-Ethyl-3-methylimidazolium bis(trifluoromethylsulfonyl)imide
$[EMIM]^+$	1-Ethyl-3-methylimidazolium cation
$[NTf_2]^-$	Bis(trifluoromethylsulfonyl)imide anion
AC	Activated carbon
B3LYP5	Becke's three-parameter and Lee–Yang–Parr functional
CAM–B3LYP	Coulomb–Attenuating Method Becke–Lee–Yang–Parr
C_s	Specific capacitance of electrode
CV	Cyclic Voltammetry
DFT	Density functional theory
EIS	Electrochemical impedance spectroscopy
E_g	Energy gap
E_T	Coulombic energy of interaction
F	Faraday constant
FRA	Frequency Response Analysis
GAMESS	General Atomic and Molecular Electronic Structure System
HOMO	Highest Occupied Molecular Orbital
HPLC	High performance liquid chromatography
IL	Ionic liquid
IILs	Imidazolium based Ionic Liquids
$K_p(T)$	Equilibrium constant
LED	Light emitting diode
LUMO	Lowest Unoccupied Molecular Orbital
MOs	Molecular Orbitals

NMP	N-Methyl-2-pyrrolidone
PGSTAT	Potentiostat-Galvanostat
PVDF	Polyvinylidene fluoride
$Q_{i,j}$	Mulliken charge
SC	Supercapacitor
$\Delta_r E$	Energy of the reaction
$\Delta_r H°(0)$	Enthalpy of the reaction
$\Delta_r \varepsilon$	Zero-point vibration energy
$\Delta_r \Phi°(T)$	Reduced Gibbs free energy of the reaction
ε(MO)	Energy of the molecular orbital
ε_o	Electric constant
$\Sigma\omega_{i\ prod}$	Sum of the vibration frequencies of the product
$\Sigma\omega_{i\ react}$	Sum of the vibration frequencies of the reactants

CHAPTER ONE

INTRODUCTION

1.1 Background of the problem

Supercapacitors (SCs) are energy storage devices that have promising energy loading capacity. The mechanism of storing energy is based on the separation of electrolyte ions, and their accumulation on the electrode surfaces with opposite charges (Forse, Merlet, Griffin & Grey, 2016; Salanne *et al.*, 2016). SCs exhibit high power densities due to their capability of being fully charged and discharged within seconds and they possess low equivalent series resistance (Vatamanu, Vatamanu & Bedrov, 2015; Kondrat & Kornyshev, 2016). The scientific and technological significance of ionic liquids now spans a wide-range of applications in energy storage and conversion (Wang, Song & Xia, 2016). In energy storage devices like supercapacitors, ionic liquids can replace the conventional aqueous solutions and organic solvents as electrolytes. This is attributed due to their large electrical potential window under electrochemical operation and their appropriate ionic sizes to pore sizes of electrode materials (Largeot *et al.*, 2008; Welton, 2018).

Ionic liquids are molten salts that possess excellent electrochemical stability and conduct at room temperature without the presence of solvents. They are considered as green liquids due to the range of their physical properties like high thermal stability at room temperature and the extent of temperatures between the freezing point and boiling point of a liquid; from –80 °C to ≥ 250 °C (Balducci *et al.*, 2007; Lin *et al.*, 2011; Ruiz, Huynh, Sivakkumar & Pandolfo, 2012). Optimisation of electrolytes materials moves parallel with the right choice of electrode materials with which the electrode-electrolytes interaction should result into production of high energy density (Pandolfo & Hollenkamp, 2006; Xu, Xiao, Zhang, Wang & Zhang, 2009). The effect of electrochemistry taking place between electrode and electrolyte has excellent impact to the performance of electrochemical cell (Bard *et al.*, 1993; McCreery, 2008; Simon & Gogotsi, 2010) due to the fact that the internal resistance and capacitive behaviour of the cell generate at the interface of the two active materials. Figure 1 shows the graphical representation of the interaction between the electrode and electrolyte at the interface.

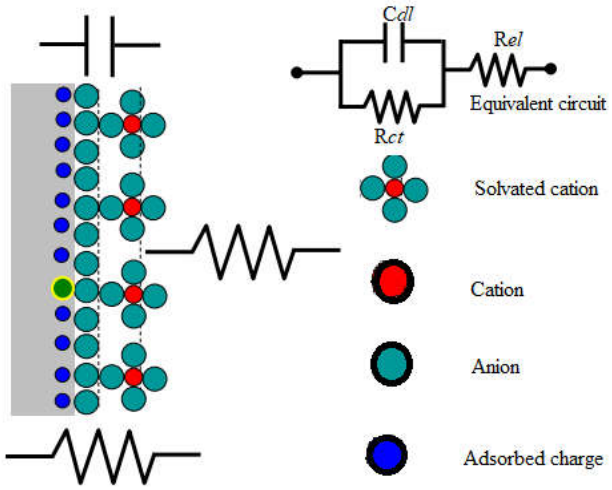

Figure 1: Schematic diagram showing the equivalent electrical circuit formed at the electrode-electrolyte interface (Hassibi, Navid, Dutton & Lee, 2004)

The primary materials for electrodes employed in SCs are all forms of carbon and carbon composites (Frackowiak & Beguin, 2001; Zhang & Zhao, 2009), this is due to the fact that electrodes that have designed based on carboneous materials are of great interest and they are of moderate cost, light-weight, abundant, high charge storage, easy to process, and possess high electronic conductivity (Frackowiak, 2007). The unique surface area of carbon materials can be obtained due to their versatility which enables the different nanostructures to be synthesised (Hu & Srinivasan, 2001; Bleda-Martínez *et al.*, 2005), rendering a wide range of physical properties suitable for energy storage applications. All types of carbon materials have been used to develop different type of energy storage devices and have performed well; these include carbide-derived carbons, carbon nanotubes, onion-like carbons, carbon fabrics, graphene nanohorn carbons and templated carbons (Pandolfo & Hollenkamp, 2006; Zhai *et al.*, 2011; Jiang, Lee & Li, 2013).

Understanding the partial charge transfer process between the carbon materials and adsorbed ions is an essential feature for electrochemical systems (Ni & Li, 2016; Eftekhari, 2018). This process has a repercussion on the mechanism of energy storage in supercapacitors which is related to the formation of a double electric layer at the electrode/electrolyte interface. It has been shown by Siimenson *et al.* (2016) and Martins and Torresi (2018) that in addition to typical electrostatic interactions in the electrical double-layer of the supercapacitor; the quick faradaic redox reactions with electron transfer on the electrode/electrolyte interface enhance energy through the contribution of the charge-storage process. Experiments show that imidazolium ionic liquids play an active role in raising the energy density of supercapacitor (Lian *et al.*, 2016). In comparison to other electrolytes, imidazolium ionic liquids have high

conductivity, high electrochemical stability and low viscosity, which are considerable influence for the performance of electrochemical capacitor electrolytes (Maiti, Pramanik & Mahanty, 2015; Pal & Ghosh, 2018). The integration of imidazolium ionic liquids in energy storage systems is a new technology which has potential use in solving severe problems of low energy density in electrochemical capacitor related to electrical energy storage for a wide range of applications.

Several technologies employing the different kinds of electrolytes and electrode materials for supercapacitor development have been reported such as alkali based supercapacitor technology, organic and aqueous-based electrolyte supercapacitor design (Stoller & Ruoff, 2010; Andres *et al.*, 2012). However, all these materials and approaches have disadvantages, such as substantial investment costs, or operating in limited temperature range, low conductivity, high viscosity, toxic and difficulties in materials preparation (Johns, Roberts, Wakizaka, Sanders & Owen, 2009; Fic, Meller, Menzel & Frackowiak, 2016). This study aims at investigating the potential of imidazolium based-ionic liquids as electrolytes with high breakdown voltage for the development of electrochemical capacitor. Imidazolium ionic liquids are purchasable, and activated carbon materials are readily available.

1.2 Statement of the problem

The production of electrochemical energy storage devices like supercapacitors is under serious consideration as an alternative for powering many electrical devices (Pilathottathil, Thasneema, Thayyil, Pillai & Niveditha, 2017). The consumption of this energy is designed to be more sustainable and more environmentally friendly due to the fact that it will be stored in cheap, harmless materials and operating at high temperature range compared to other materials which are reported to be expensive, poisonous, tedious requiring much attention due their explosiveness (Dyatkin *et al.*, 2018). Any electrochemical device that is environmentally friendly is the result of the right choice of its components like electrodes and electrolytes. Imidazolium based ionic liquids are among the green solvents that mimic the stable electrolytic behaviour for supercapacitive energy storage. Although several studies (MacFarlane *et al.*, 2016; Mousavi *et al.*, 2016) have reported the supercapacitive performance of imidazolium based ionic liquids (IILs) with AC electrodes, the thermodynamic characteristics of IILs that contribute to the SC performance have not yet explored. Therefore, there is a need to study the thermodynamics of IILs and to determine the

electrochemical performance exhibited by IILs using Density Functional Theory (DFT), Cyclic Voltammetry (CV) and Electrochemical Impedance Spectroscopy (EIS) methods.

1.3 Rationale of the study

Energy storage for fast back up in delicate devices like electronics and load-leveling during the time of over-power production is the most challenge facing the digital world, this challenge move parallel with the fast depletion of the bulky energy from the fossil fuel. Alternative technologies have been employed like fuel cells and lithium-ion batteries to address the problem while meeting the protocols on environmental protections (Yang *et al.*, 2011; Choi *et al.*, 2012). The electrochemical cells (supercapacitors) of low cost, high power density, easy to fabricate and utilizing locally available materials that have no harm to environments, have become a viable solution to a problem of extreme energy intermittent compared to other energy storage devices with complications in manufacturing and being expensive.

1.4 Objectives

1.4.1 General objective

The general objective of this study is to investigate the potential of imidazolium-based ionic liquids for supercapacitors application.

1.4.2 Specific objectives

(i) To determine the structural and thermodynamic properties of imidazolium-based neutral ion pairs by using quantum chemical computations.

(ii) To examine the performance of the electrochemical capacitor utilising imidazolium-based ionic liquids as electrolyte and available activated carbon electrode materials.

1.5 Research questions

(i) What are the structural and thermodynamic properties of imidazolium-based neutral ion pairs?

(ii) What is the performance of imidazolium-based ionic liquids in enhancing the energy density in the electrochemical capacitor?

1.6 Significance of the study

Energy storage plays a substantial role in massive growth of renewable energy sources. Due to intermittent and unpredictable nature of power generation, energy storage needs to be used to ensure that the electrical loads are met at all times. The use of an electrochemical capacitor as the storage device will enhance more options to proper utilisation of energy after being generated.

1.7 Delineation of the study

The study was both theoretical and experimental, whereby the neutral ionic pairs in gaseous phase were studied based on their coulombic interaction as well as thermodynamic stability. The theoretical approach utilized computational software for investigating the physical properties like the HOMO-LUMO energies which helped to predict the potential window of the ionic liquids when treated as electrolyte. With the support of activated carbons, the experimental part was conducted at room temperature to investigate the electrochemical properties of ionic liquids like specific capacitance, ionic impedance, energy and power density by using cyclic voltammetry and electrochemical impedance spectroscopic method. Finally, the electrochemical capacitor utilising ionic liquids was fabricated and tested.

CHAPTER TWO

LITERATURE REVIEW

2.1 Introduction

The significant role of storage performance in a supercapacitor is played by the active participation of the electrolyte and electrode in collaboration with the passive components of the supercapacitor like the current collector, separators and binder (Shen, Wang, Zhang & Kang, 2011). The supercapacitors can be classified based on the electrode materials with their mode of charges/ions storage as well as the electrochemical inertness of the electrode (Huggins, 2000; Wang, Yan & Fan, 2016).

2.2 Working principle of supercapacitors

A supercapacitor is an energy storage device having the electrodes for potential charge storage and electrolyte for providing ionic conductivity between electrodes as shown in Fig.2. Energy storage capacity of the supercapacitor is defined by its specific capacitance and cycle stability during charging and discharging.

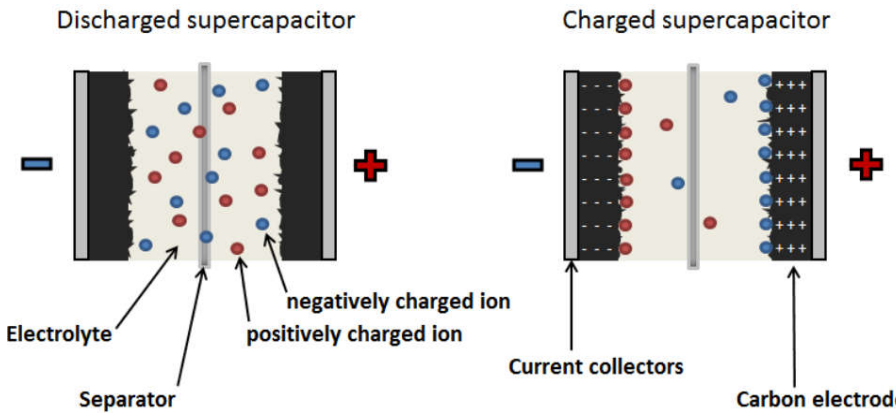

Figure 2: Schematic diagram showing the working principle of a supercapacitor (Vuorilehto & Nuutinen, 2014)

Generally for a supercapacitor to work, the electrolyte must play an initial role whereby the transformation of faradaic reaction into electrical energy is involved according to the equation, $E = -n\,F\,V$; where E represents a performed work in J mol^{-1}, n is the number of electrons that have been transferred, F stands for Faraday constant and V represents the change in voltage. When the supercapacitor is not charged, the ions are evenly distributed in the way that the electrochemical cell is at rest potential. The electric double layer is formed at

the interface as the result of applied voltage, the opposite charges are created on both sides of the separator, and the metal substrates get charged.

2.3 Electrode materials for supercapacitors

The choice of electrode materials acts as the guide towards the development of the supercapacitor (Yu & Chen, 2016). There is a possibility for a supercapacitor to possess mainly a double-layer capacitance, which is the characteristic of all forms of carbon materials with the charge storage appearing only as electrostatic accumulation of the charges on the surface of electrode materials. Another property exhibited by other types of supercapacitors is pseudocapacitance, which is portrayed by oxides of transition metals and conductive polymer materials having the behaviour of faradaic charge storage, whereby redox reaction mechanism takes place on the surface of electrode materials (Libich, Máca, Vondrák, Čech & Sedlaříková, 2018; Miller, Hua & Tezel, 2018). From a double layer capacitance and pseudocapacitance, the third category forms which is the hybrid capacitance of the supercapacitor as the result of the combination of conventional electrode materials to produce composite materials which exhibit charge storage electrostatically as well as faradaically (Godillot *et al.*, 2016; Li *et al.*, 2016).

The emergence of nanotechnology was a game-changer to the field of energy storage since it facilitated the synthesis and production of electrode materials at nanoscale, which have fast charging mechanism and high power storage (Liu, Kopold, van Aken, Maier & Yu, 2015; Deng, Lu, Liu, Zhang & Schmidt, 2016; Lu *et al.*, 2016; Zeiger, Jäckel, Mochalin & Presser, 2016). The carboneous electrode materials are the ones that are highly researched currently, and this has no doubt that they possess exceptional chemical stability, electrical conductivity, low manufacture and processing cost large surface area, high-temperature tolerance and they are environmentally friendly (Khan, Saeed & Khan, 2017). The resulting product from the synthesis of the carbon-based electrode materials can be porous or nonporous. The porous carbon materials include activated carbons which appears with the most considerable advantage over non-porous for supercapacitor application, simply because porous carbon as electrode materials have reasonable specific surface area which results into high capacitance values in comparison to other carboneous materials like carbon nanotubes (Frackowiak, 2007; Jiang *et al.*, 2015).

2.4 Types of electrolytes used in electrochemical cells

Electrolytes initiate the electrical energy in electrochemical cells by allowing the chemical reaction in it (Jiang, Hu, Yan & Wu, 2017). The conversion of chemical energy to electrical energy occurs in electrolytes before passing to the surface of the electrode (Singh, Rakib, Chavhan & Ganguly, 2016). With these critical initiatives in the electrolyte, makes the electrolytes act as the heart of the electrochemical system. Electrolytes that are used in energy storage devices are categorised as aqueous, organic and ionic liquids based electrolytes (Laheäär, Przygocki, Abbas & Béguin, 2015; Balducci, 2016).

Soluble acids like H_2SO_4 and alkalis with high ionic conductivity have been used in energy storage devices despite being limited by their electrochemical potential window. They are capable of generating high specific capacitance of around 390 F g^{-1} (Sudhan, Subramani, Karnan, Ilayaraja & Sathish, 2016; Karnan, Subramani, Srividhya & Sathish, 2017), when combined with the electrodes activated carbon-based electrode materials. Organic electrolytes are generally more preferred due to their higher operating potential although they are limited by faster electrochemical decomposition process and volatility factors that make them to operate in a limited range of temperature (Fic *et al.*, 2016; Yu, Lu, Zheng & Lu, 2018). Figure 3 shows the exponential dependence of the energy density on the potential window for three classes of electrolytes.

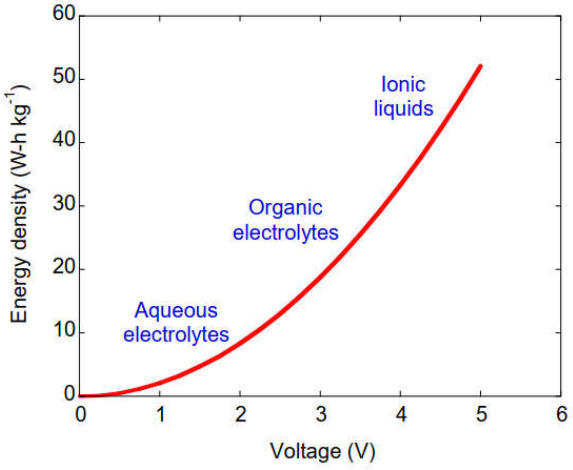

Figure 3: Sketch showing the dependence of energy density on the operating voltage of electrolytes (Lin, 2012)

Recent studies of ILs survey the chemical and physical properties which are of scientific and technological significance (Vyas *et al.*, 2014; Watanabe *et al.*, 2017; Yoo, Pu & Ragauskas,

2017; Kar, Plechkova, Seddon, Pringle & MacFarlane, 2019). Researchers report that physicochemical characteristics of ionic liquids are governed by coupling between positively and negatively charged species, special hydrogen bonding, short-range and long-range interactions (Dhumal, Noack, Kiefer & Kim, 2014; Low, Tan & Pas, 2019). Wide-range of applications of ILs are based on characterising them as designer solvents for gas or liquid separation processes, lubricants for reducing wear and tear in machine parts, for separating agents, chemical reactions, and electrolytes for high-efficiency electrochemical devices like electrochemical sensors (Wei & Ivaska, 2008; He & Alexandridis, 2015; Eshetu, Armand, Ohno, Scrosati & Passerini, 2016; Eftekhari & Saito, 2017; Watanabe *et al.*, 2017; Yoo *et al.*, 2017). In energy storage devices like supercapacitors, ionic liquids as electrolytes show promising features in raising energy in supercapacitors (Van Aken, Beidaghi & Gogotsi, 2015; MacFarlane *et al.*, 2016). With the ongoing researches, room temperature ionic liquids replace the conventional aqueous solutions and organic solvents in many energy storage devices (Salanne, 2017; Watanabe *et al.*, 2017).

Imidazolium based ionic liquids are among the first ILs investigated experimentally (Welton, 2018; Danielewicz, Kmiotek & Surma-Ślusarska, 2019). Since the properties ILs can be altered by modifying the initial structure of anion over the same positively charged part, a variety of anions such as bis(trifluoromethylsulphonyl)imide ion (NTf_2^-), bis(fluorosulfonyl)imide ion (FSI^-), hexafluorophosphate ion (PF_6^-), dicyanamide ion (DCA), tetrafluoroborate ion (BF_4^-) chloride ion (Cl^-), bromide ion (Br^-) (Rogers & Seddon, 2003; Chiappe & Pieraccini, 2005; Dong, Liu, Dong, Zhang & Zhang, 2017), among others have been manipulated to come up with IL species having different physicochemical properties for extensive applications (MacFarlane *et al.*, 2014; Mousavi *et al.*, 2016). Such focus of exchanging cations and anions brings new knowledge of expanding the field of ionic liquids by establishing the link between structures and new and practically demanding properties of ILs.

Quantum chemical and molecular dynamic studies of the structural and thermodynamic properties of ionic liquids should be taken into account as they bring new insights on how ionic liquids interact themselves as well as with other materials (Liu, Sale, Holmes, Simmons & Singh, 2010; Janesko, 2011; Merlet *et al.*, 2012). This is because the study of the influence of dispersion forces, charge distribution in molecular orbitals, electrostatic interaction and parameters like structural changes at molecular level is required (Weingärtner, 2008; Wu,

Jiang, Jiang, Jin & Henderson, 2011; Ray, Elfgen & Kirchner, 2019) so as to survey the physicochemical properties, which are responsible to give theoretical values that accord with experimental values (Hunt, Gould & Kirchner, 2007; Cho *et al.*, 2011). Studies in quantum chemical calculations authenticate that the potentiality of the ionic liquids originates from molecular grounds making them suitable electrolytic candidates for raising energy in supercapacitor and other energy storage devices (Jiang, Meng & Wu, 2011; Weingarth *et al.*, 2012).

2.5 Current status of supercapacitors utilising ionic liquids

Since the time when supercapacitors were developed as an alternative for energy storage, a new type of electrolyte (ionic liquids) came to take over the role of connecting the electrodes by providing ionic conductivity to the electrochemical cell and attracted considerable attention (MacFarlane *et al.*, 2016; Mousavi *et al.*, 2016) due to their advantage of being environmentally friendly and thermodynamically stable. Currently, effort and focus in supercapacitor researches have been placed into coming up with new ways of improving local materials for better electrode properties to boost the performance of the supercapacitor (Yu *et al.*, 2017; Lin *et al.*, 2018).

Activated carbon electrodes, apart from their precursors being locally available and having a low cost of production (Wei, Wei, Gao & Li, 2015), have shown their strength in raising the specific capacitance of the supercapacitor. Unlike graphene and MXene, which have a high cost of production and are under (Xin & Yu, 2017; Wang *et al.*, 2018) low production rate hinder the practical use of these materials in expanding supercapacitor technology. Hence activated carbons still met the requirements to be integrated into developing the electrochemical systems for mass production of energy storage devices. Compared to the supercapacitor based on conventional electrolytes, supercapacitors based on ionic liquids as electrolytes belong to the current generation of energy storage devices that can be used to power electrical and electronic systems. Therefore, due to thermodynamic and kinetic stability of ionic liquids, the supercapacitor utilising ionic liquids are capable of working under moist environment and wide range of temperature (Zhang, Tsay, Bock & Zhang, 2016; Salanne, 2017), whereas organic electrolyte-based supercapacitors would suffer from electrolytic degradation at some high-temperature exposure.

CHAPTER THREE

MATERIALS AND METHODS

3.1 Introduction

This chapter introduces the computation methods used get optimized geometries of both ionic liquids which late helped to determine the thermodynamic functions of the electrolyte materials. It highlights also the originality of materials used in the research, the procedures undertaken during the entire lab work for preparation of activated carbon electrode and IILs solutions. The electrochemical study was achieved through carrying out cyclic voltammetry and frequency response analysis method.

3.2 Theoretical computations details

The initial coordinates of charged species of the $[EMIM]^+$ cation, $[BF_4]^-$ and $[NTf_2]^-$ anions were retrieved from ChemSpider Database (Meredith, 2012) and neutral ion pairs $[EMIM][BF_4]$ and $[EMIM][NTf_2]$ from The Cambridge Structural Database (Groom, Bruno, Lightfoot & Ward, 2016). To ensure that the outputs corresponded to stable conformers, the geometrical structures optimisation was performed without any constraint of resulted geometry as well as the vibrational harmonic frequencies computed. The DFT method with Becke-Lee-Yang-Parr functional (B3LYP5) alongside with Coulomb-Attenuating Method Becke-Lee-Yang-Parr functional (CAM-B3LYP) combined with Pople type basis sets of 3-21G(d,p), 6-31G(d,p), 6-311G(d,p) and 6-311++G(d,p) in FireFly QC program (Granovsky, 1994-2018) on the GAMESS (US) source code (Schmidt *et al.*, 1993) and ORCA Program System (Neese, 2012) was used. The optimized geometrical structures, vibrational spectra of the species and ground state isodensity surfaces of frontier molecular orbitals were visualised, plotted and analysed using the Chemcraft (Zhurko & Zhurko, 2015) and MacMolPlt software (Bode & Gordon, 1998).

The thermodynamic functions of the gaseous species have been calculated on the basis of optimized geometrical parameters and vibrational frequencies in 'rigid rotor-harmonic oscillator' approximation by means of OpenThermo program (Tokarev, 2007–2009). The energies and enthalpies of inter-ionic reactions $\Delta_r H°(0)$ were calculated theoretically through the total energies of the participants. For the $[EMIM][NTf_2]$, the treatment of the

experimental data available in (Dunaev, Motalov, Kudin & Butman, 2016) was done by using our thermodynamic functions.

3.3 Materials and reagents collection

The ionic liquids of 1-ethyl-3-methylimidazolium tetrafluoroborate ([EMIM][BF_4]) and 1-ethyl-3-methylimidazolium bis(trifluoromethylsulfonyl)imide ([EMIM][NTf_2]) samples were purchased with a stated purity of 98% (High-performance liquid chromatography-HPLC Standard) from Sigma-Aldrich Chemical Company (Switzerland), and were prepared to form dilute solutions and used as electrolytes at room temperature. Other auxiliary materials like polyvinylidene fluoride (PVDF) in powder form and N-Methyl-2-pyrrolidone (NMP) with American Chemical Society grade reagent of 99.0% were purchased from Sigma-Aldrich Chemical Company (Switzerland). Copper and nickel foams as metal substrate were purchased from Shanghai Tankii Alloy Material Co, Ltd. All materials were used without extra refinement.

3.4 Preparation of activated electrode materials

The fabrication of electrodes was carried out by considering the formation of the slurry, which was developed by mixing activated carbon with the specific surface area of 1294.872 $cm^2\ g^{-1}$ with the mesopore and micropore volume of 0.4955 and 0.253 $cm^3\ g^{-1}$ (Sufiani, 2019), Polyvinylidene fluoride (PVDF) and carbon black. The working electrode was prepared by mixing 70 wt% activated carbon, 10 wt% PVDF binder and 20 wt% carbon black in Petri dish. A suitable amount of N-Methyl-2-Pyrrolidone (NMP) was put to the mixture to form slurry, which was subsequently smeared on nickel foam and dried in an oven at 150 °C for 2 hours. An excellent mechanical strength was shown by the fabricated electrodes as there was no detachment of carboneous materials upon rubbing.

3.5 Preparation of electrolytes

Acetonitrile was used as a solvent, from the stock solution of 3.8 M of [EMIM][NTf_2] and 6.4 M of [EMIM][BF_4], 2 M of each component were prepared independently to form dilute solutions. Acetonitrile was chosen to be used for dilution of both ionic liquids due to its ability to dissolve a wide range of solute and capability to conduct electricity at room temperature.

3.6 Electrochemical measurements

Electrochemical studies were performed in the three-electrode system at room temperature. The activated carbon on nickel substrate was set as the working electrode, platinum rod and silver-silver chloride were employed as counter and reference electrodes respectively, in 2 M of ionic liquids of [EMIM][BF_4] and [EMIM][NTf_2]. The voltammograms of the electrochemical system prepared have been recorded in the potential range of –1.2 V to 1.6 V using a Potentiostat Galvanostat machine – PGSTAT204 (Metrohm Autolab - AUT 50663) with the help of NOVA software (NOVA 1.11) as shown in Fig. 4. The electrochemical impedance spectra were measured using the Frequency Response Analyser (FRA), an integral part of the PGSTAT204. Excel and OriginLab software were used for further processing and analysing of the data.

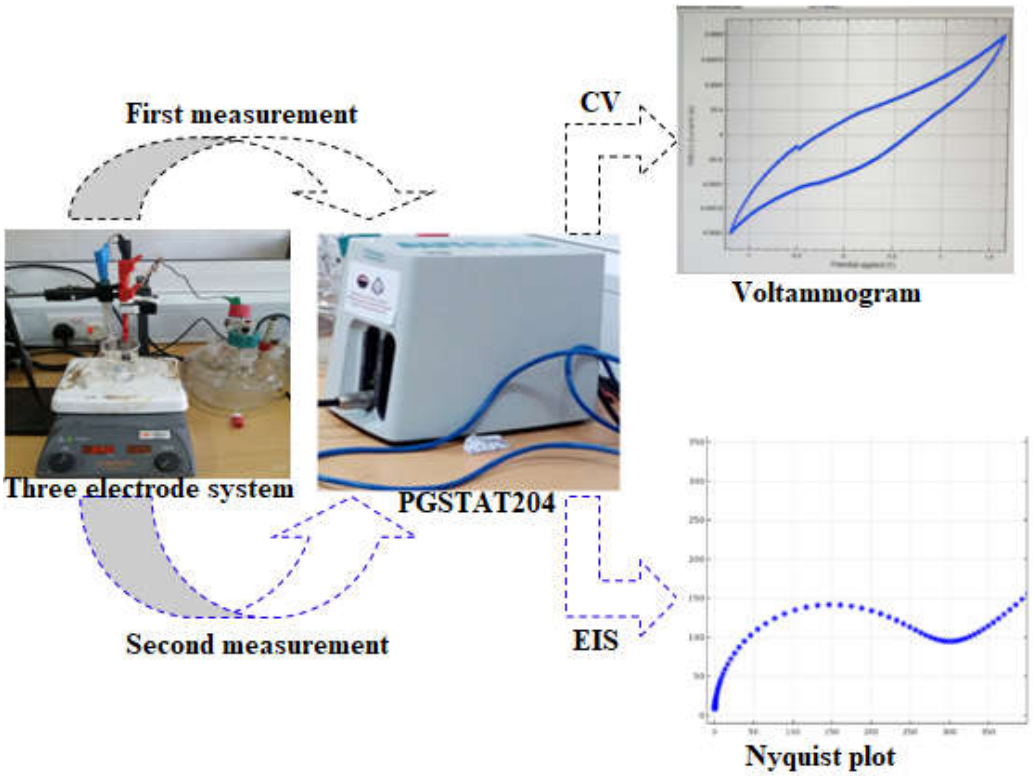

Figure 4: CV and EIS measurement

3.7 Fabrication of the supercapacitor prototype

The activated carbon electrodes on copper and nickel foam substrates were fired at 150 °C for 2 hours in the oven and then left to cool in atmospheric air. The dried activated carbon electrodes were rinsed with ethanol to get rid of loosely attached carbon materials on

electrodes and then dried in air to leave ethanol to evaporate. The supercapacitor prototype was designed by slotting two electrodes (copper and nickel foam substrates with the dimension of 3 cm by 3 cm) separated by a Whatman separator soaked with electrolyte of [EMIM][NTf_2] and [EMIM][BF_4]. The assembling of supercapacitor cell was carried out as shown in Fig. 5.

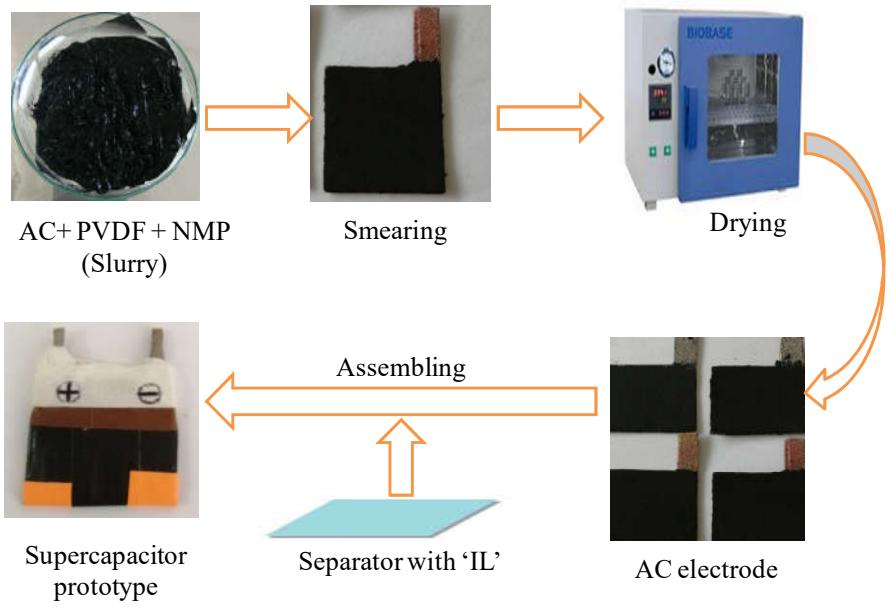

Figure 5: Assembling of supercapacitor cell

3.8 Conventional charge-discharge measurement of supercapacitor prototype

The charging and discharging test of the prototype was done by setting up protoboard to which other electrical components like battery, resistor and multimeter were connected as shown in Fig. 6. The trend of charging and discharging behaviour was recorded by using a stopwatch.

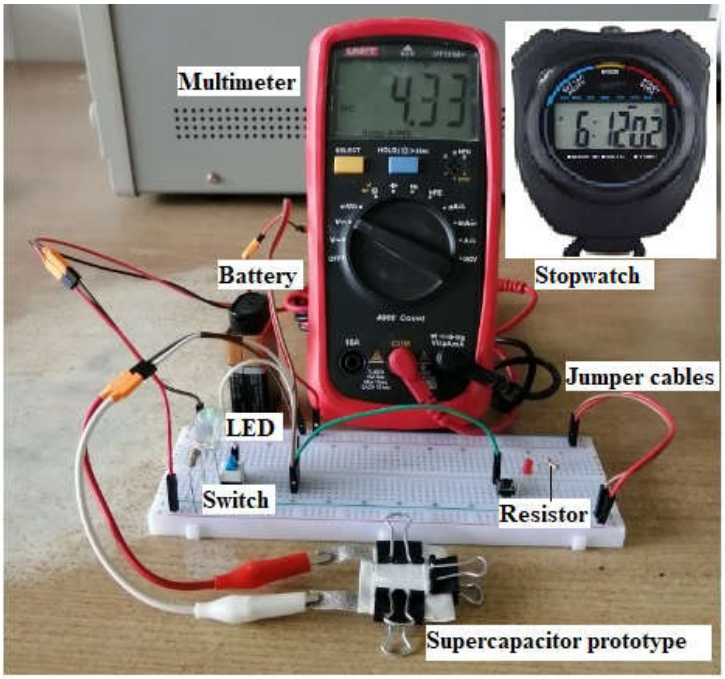

Figure 6: Experimental setup for conventional charge-discharge measurement of supercapacitor prototype

CHAPTER FOUR

RESULTS AND DISCUSSION

4.1 Introduction

This chapter presents and confers about the theoretical optimization of imidazolium based ionic liquids as electrolyte materials for electrochemical cells. It illustrates the performance of the optimized electrolytes in producing the parameters of the electrochemical system. The interaction between activated carbon electrodes and electrolytes was tested at different scan rates, the generated voltammograms, specific capacitances and electrochemical impedance spectra were analysed.

4.2 The optimised geometrical structure of charged ions and neutral ion pairs

Equilibrium geometries of $[EMIM]^+$ cation, $[BF_4]^-$ and $[NTf_2]^-$ anions are shown in Fig. 7. The combination of two ions through inter-ionic reactions may be considered:

$$[EMIM]^+ + [BF_4]^- = [EMIM][BF_4] \quad (1)$$

$$[EMIM]^+ + [NTf_2]^- = [EMIM][NTf_2] \quad (2)$$

The reactions result in the production of the ion pairs $[EMIM][BF_4]$ as well as $[EMIM][NTf_2]$. The conformational search of neutral pairs allows choosing the conformers with the lowest energy. It has been reported also in (Tsuzuki, 2005; Paulechka, Kabo & Emel'yanenko, 2008; Katsyuba, Griaznova, Vidis & Dyson, 2009), that the ion pairs can form different conformers as result of combination of different moieties of *cis*- and *trans*-forms of charged species forming the pairs with minima on the potential energy surfaces. Thus in the case of the $[EMIM][NTf_2]$, the stable configuration occurs when the *trans*-conformer of anion (Fig. 7c) is positioned under the plane of the imidazolium ring near the C1 atom (Fig. 7a). The ion pairs with the lowest energies were considered, and their geometries are displayed in Fig. 8.

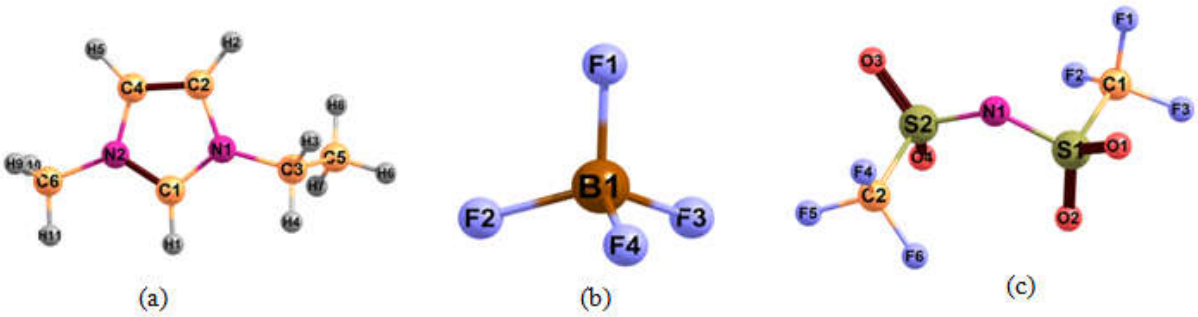

Figure 7: The optimized geometrical structures of charged chemical species: (a) $[EMIM]^+$ cation, (b) $[BF_4]^-$ anion, (c) $[NTf_2]^-$ anion

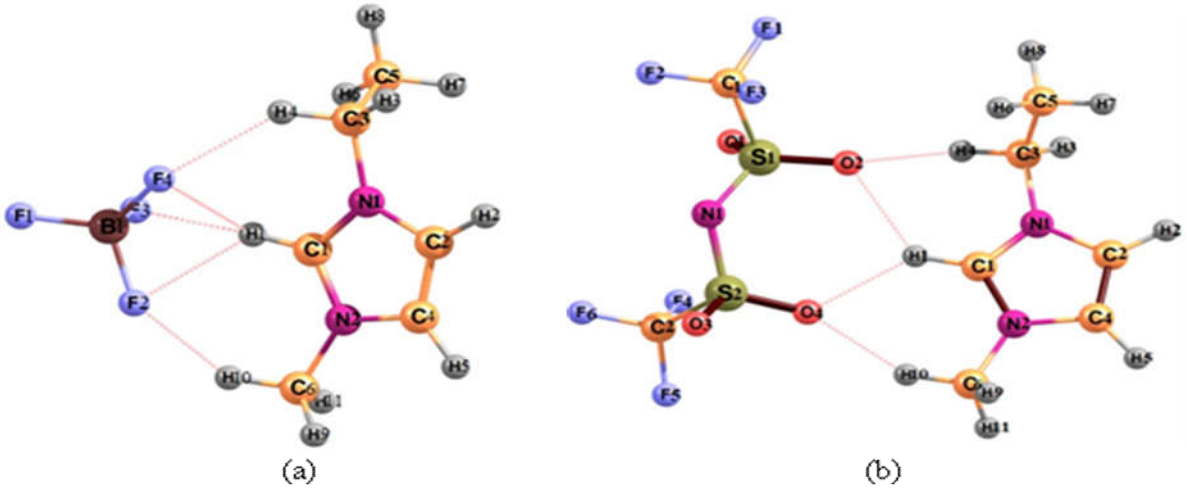

Figure 8: The optimized geometrical structures of ionic pairs: (a) $[EMIM][BF_4]$, (b) $[EMIM][NTf_2]$

The ionic pairs are coupled by strong Coulombic forces and hydrogen bonding whereby in the $[EMIM][BF_4]$, the inter-atomic separations F…H are in range 1.99-2.26 Å, in the $[EMIM][NTf_2]$, four hydrogen bonds are formed with O…H separations 2.11-2.20 Å. The selected relevant geometrical parameters of free ions and ion pairs are compared and arranged in Table 1; for the neutral species, the comparison of simulated values with available experimental X-ray diffraction data (Matsumoto, Hagiwara, Mazej, Benkič & Žemva, 2006; Paulechka *et al.*, 2009) was performed.

As can be seen, among the cation bonds C1-H1, C3-H4 and C6-H11 which are involved into links with anions forming the ion pairs, only the central one, C1-H1, is elongated slightly (by 0.007 Å), while the other two remain almost unchanged. As for the anion $[BF_4]^-$, a remarkable change of the B-F separation occurs when the molecule $[EMIM][BF_4]$ is formed; from 1.417 Å to 1.374, 1.440, 1.424 and 1.425 Å; the angles F-B-F are also changed from tetrahedral (109.5°) by ±3°. In the $[NTf_2]^-$ anion, the bonds S-O which participate in the linkage are elongated by 0.014 Å, while the diverted S-O bond is contracted by 0.012 Å. The

change in the bond lengths is accompanied with significant variation of bond angles C-S-N and O-S-N, by 6-7°. The other bonds and angles remote from the links are not altered noticeably in the molecules compared to the free cation or anions.

Table 1: Comparison of selected geometrical parameters between free ions $[EMIM]^+$, $[BF4]^-$, $[NTf_2]^-$ and respective neutral ionic pairs computed at B3LYP5/6-311++G(d,p)

Parameter	$[EMIM]^+$	$[BF_4]^-$, $[NTf_2]^-$	[EMIM][BF_4]		[EMIM][NTf_2]	
Bond lengths, Å	Calc	Calc	Calc	Expt [37]	Calc	Expt [36]
N1-C1	1.329		1.328	1.328	1.331	1.314
N1-C2	1.377		1.378	1.381	1.377	1.356
N1-C3	1.477		1.476	1.469	1.474	1.482
N2=C1	1.330		1.328	1.320	1.331	1.326
N2-C4	1.377		1.378	1.382	1.377	1.366
N2-C6	1.465		1.462	1.466	1.466	1.474
C2=C4	1.354		1.353	1.350	1.353	1.349
C3-C5	1.519		1.516	1.505	1.518	1.458
C1-H1*	1.078		1.085*		1.085*	
C3-H4*	1.091		1.091		1.088*	
C6-H11*	1.088		1.089		1.088*	
B1-F1		1.417	1.374	1.385		
B1-F2*		1.417	1.440*	1.398		
B1-F3		1.417	1.424	1.385		
B1-F4		1.417	1.425	1.400		
C1-F1		1.340			1.323	1.313
C1-F2		1.348			1.344	1.319
C1-F3		1.339			1.343	1.313
C1-S1		1.891			1.890	1.838
S1-O1*		1.464			1.478*	1.419
S1-O2		1.465			1.453	1.431
S1-N1		1.617			1.603	1.579
Bond angles, deg	Calc	Calc	Calc	Expt [37]	Calc	Expt [36]
C2-N1-C1	108.3		108.6	108.3	108.7	108.6
C3-N1-C1	125.8		125.1	125.2	125.7	124.8
N1-C1=N2	109.0		108.7	109.0	108.5	108.6
H1-C1-N1	125.5		125.7	125.4	125.9	125.7
N2=C1-H1*	125.5		125.6*	125.5	125.5*	125.7
C2-N1-C3	125.8		125.7	126.5	125.6	126.6
C4=C2-N1	107.2		107.1	107.1	107.0	107.8
C2=C4-N2	107.1		106.9	106.8	107.1	106.1
C1=N2-C6	126.0		124.3	125.7	125.8	125.1
C5-C3-H3	111.8		111.6	109.4	111.9	108.6
C5-C3-H4	111.5		110.1	108.8	110.1	108.5
C3-C5-H6	109.2		110.8	109.8	109.1	109.5
H3-C3-H4	107.5		109.8	108.0	109.2	107.7
C4=C2-H2	130.6		131.0	126.6	130.8	127.0
C2=C4-H5	130.7		130.8	126.5	130.9	126.1
F1-B1-F2*		109.4	111.3*	109.6		
F1-B1-F3		109.5	112.0	110.8		
F1-B1-F4		109.5	111.9	109.5		

Parameter	$[EMIM]^+$	$[BF_4]^-$, $[NTf_2]^-$	$[EMIM][BF_4]$		$[EMIM][NTf_2]$	
F2-B1-F3		109.5	106.7	109.5		
F2-B1-F4		109.5	106.6	108.5		
F3-B1-F4		109.4	108.0	108.9		
F1-C1-F2		107.7			108.8	107.8
F1-C1-F3		108.5			108.9	109.5
F2-C1-F3		107.7			108.0	107.8
F1-C1-S1		112.0			111.5	111.2
F2-C1-S1		108.3			109.2	109.4
F3-C1-S1		112.3			110.3	110.9
C1-S1-N1		95.4			102.3	102.5
S1-N1-S2		124.9			126.9	124.9
O1- S1- C1		104.4			103.1	104.3
O2- S1-C1		104.5			104.9	104.7
O1-S1-N1		114.2			115.9	116.4
O2-S1-N1		116.0			110.1	108.5

* Bonds participate in the links between cation and anion

In conjunction with the comparison of the theoretical parameters with experimental results in Table 1, the validation of simulated results is shown *via* the bar diagrams in Fig. 9, 10. For the $[EMIM][BF_4]$, the DFT methods B3LYP5/6-311G(d,p), B3LYP5/6-311++G(d,p) and CAM-B3LYP5/6-311++G(d,p) were employed in optimisation procedure. It can be seen that addition of diffusion functions improves the calculated parameters towards better accordance with the experimental data (Matsumoto *et al.*, 2006; Paulechka *et al.*, 2009) as well as with the theoretical data obtained for $[EMIM][BF_4]$ using DFT/B3LYP/6-31G* (Katsyuba, Dyson, Vandyukova, Chernova & Vidiš, 2004). Regardless of small deviations from experimental values, the geometrical parameters computed by using 6-311++G(d,p) and both DFT functionals proved to be reliable and appropriate for calculating vibrational frequencies and thermodynamic properties. The optimized geometrical parameters and vibrational frequencies of the charged species of $[EMIM]^+$, $[BF_4]^-$, $[NTf_2]^-$ and neutral ion pair of $[EMIM][BF_4]$ and $[EMIM][NTf_2]$ in gas phase at both B3LYP5/6-311++G(d,p) and CAM-B3LYP/6-311++G(d,p) methods are listed in Appendix 1 and Appendix 2 respectively.

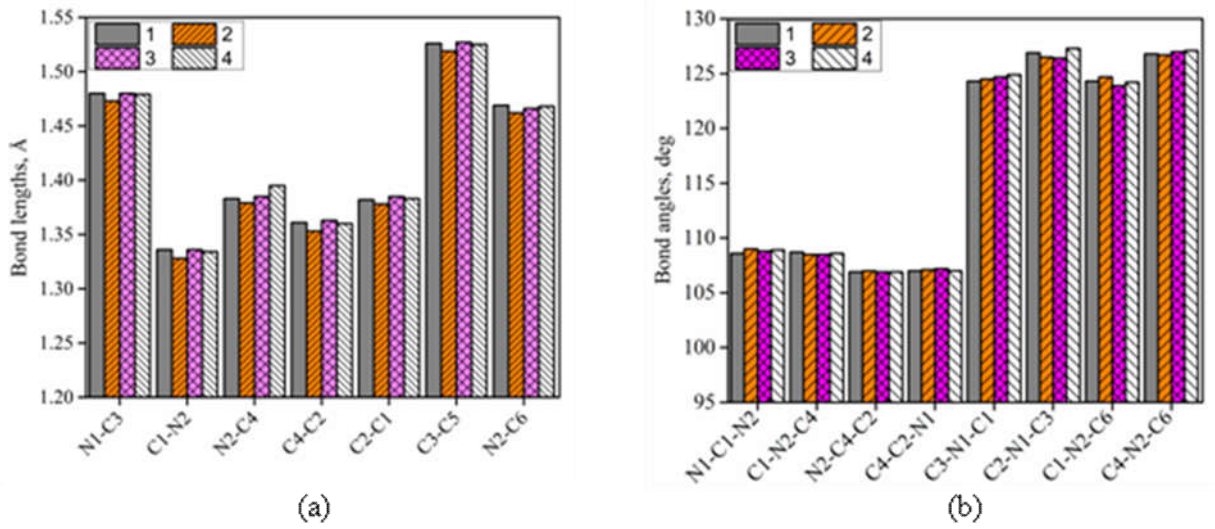

Figure 9: Comparison of calculated and experimental geometrical parameters of [EMIM][BF_4]: (a) bond lengths; (b) bond angles. In the legends, 1 – B3LYP5/6-311++G(d,p), 2 – CAM-B3LYP/6–311++G(d,p), 3 – Theoretical data (Katsyuba *et al.*, 2004), 4 – Experimental data (Matsumoto *et al.*, 2006)

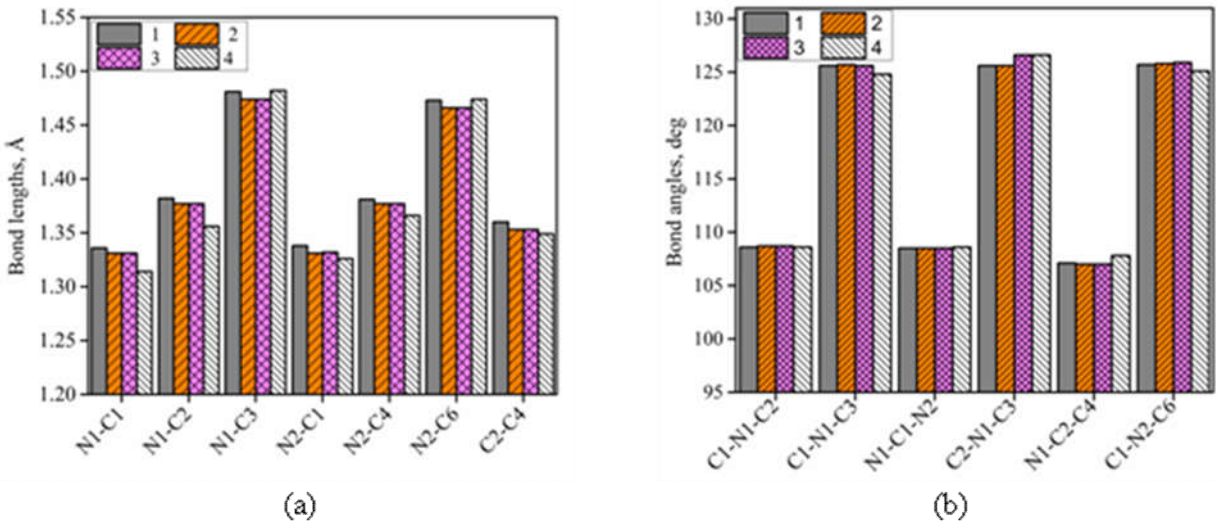

Figure 10: Comparison of calculated and experimental geometrical parameters of the [EMIM][NTf_2]: (a) bond lengths; (b) bond angles. In the legends, 1 – B3LYP5/6-311G(d,p), 2 – B3LYP5/6-311++G(d,p), 3 – CAM-B3LYP/6–311++G(d,p), 4 – Experimental Data (Paulechka *et al.*, 2009)

4.3 Frontier molecular orbitals analysis

It is with no doubt that the HOMO-LUMO energy gap is a vital parameter in finding the electrical transport mechanism of molecules. The electron density-isosurfaces over the ground state molecular orbitals of the neutral ion pairs are displayed in Fig. 11. The energy gap E_g of the [EMIM][BF_4] is rather high, 6.86 eV. The electron density of the HOMO is located at the

BF_4^- moiety, this apparently relates to the presence of highly electronegative atoms (fluorine). The distribution of charge density in the LUMO is confined on the imidazolium ring; this is due to the delocalisation of π electrons in the ring as well as the presence of electronegative atoms (nitrogen).

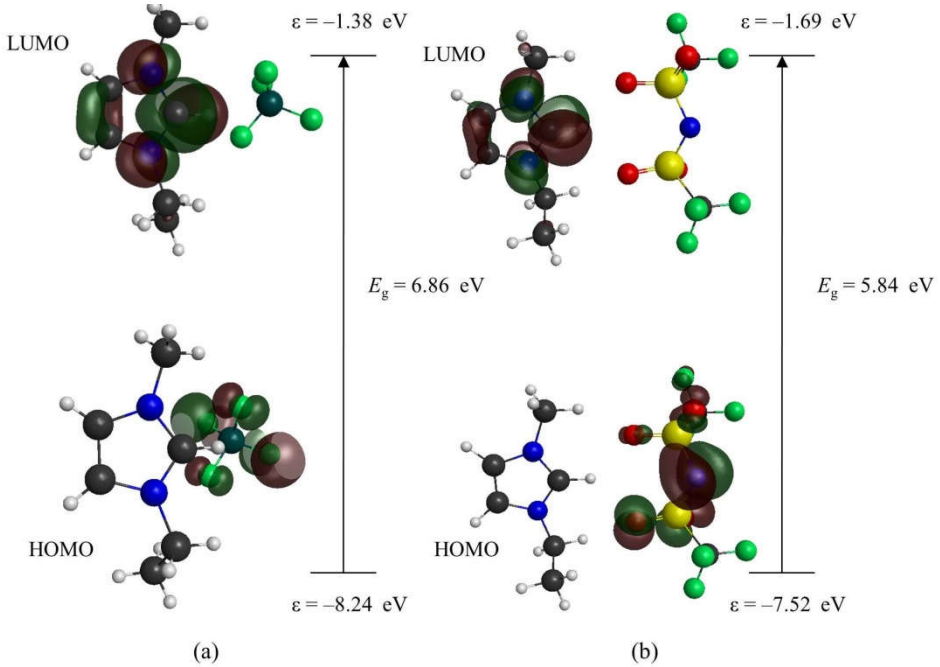

Figure 11: Frontier molecular orbitals of [EMIM][BF_4] (a) and [EMIM][NTf_2] (b)

The HOMO-LUMO energy gap of the [EMIM][NTf_2] is 5.84 eV. In the HOMO, the charge density is confined on the entire anionic part, and this is attributed to the presence of electronegative atoms, fluorine, nitrogen, sulfur and oxygen. The wider is the HOMO-LUMO gap, the more chemically stable the molecule, a property which is suitable for the material to be used as an electrolyte for energy storage application (Ong, Andreussi, Wu, Marzari & Ceder, 2011; Van Aken *et al.*, 2015).

Summarising this section, for both ion pairs, the electron density in HOMO is concentrated in the anionic moieties, while that of LUMO is located in the cationic part. The presence of negatively charged moieties in the structure of the ILs tends to raise the HOMO-LUMO energy gap that is in accordance with literature (Kazemiabnavi, Zhang, Thornton & Banerjee, 2016). The neutral ion pairs are characterised by HOMO-LUMO separation, and this is due to the existence of specified electron-rich part which is anion and electron-deficient region which is cation; hence the strong interaction in between is influenced by the charge transfer. If one compares the HOMO energies of the pairs (Fig. 11) and respective individual anions, –

4.45 eV ($[BF_4^-]$), –4.10 eV ($[NTf_2]^-$), the difference between the HOMO energies of [EMIM][BF_4] and $[BF_4^-]$ is –366 kJ mol^{-1} and between [EMIM][NTf_2] and $[NTf_2]^-$ is –330 kJ mol^{-1}. It is surprising that the HOMO energy difference between ion pair and respective anion practically coincides with the energies of the association reactions: –364 and –327 kJ mol^{-1} (Table 2). It proves that lowering of the HOMOs energies in the neutral pairs compared to pure anions occurs due to cation-anion bonding *via* Coulomb attraction.

4.4 Vibrational spectra analysis

The theoretical vibrational spectra were calculated using different approaches as detailed in the methodology. The optimised structures correspond to energy minima at the potential energy surfaces as no imaginary frequencies have been obtained hence proved the geometrical structures to be equilibrium. The simulated IR-spectra with CAM-B3LYP/6–311++G(d,p) of cation $[EMIM]^+$; anion $[BF_4]^-$, ion pairs [EMIM][BF_4] and [EMIM][NTf_2] are shown in Fig. 12. The position of most intensive peaks of the cation (Fig. 12a) is reproduced in spectra of the pairs generally, but intensities of the peaks increased noticeably (Fig. 12b, c) which probably resulted from the strong interaction between the cation and anions. In the IR-spectrum of BF_4^-, only one B-F stretching asymmetric vibration is at 1027 cm^{-1}, this vibration is seen at ~1200 cm^{-1} in the spectrum the [EMIM][BF_4] (Fig. 12b). The shift is attributed to the contraction of the B-F bond from 1.417 Å in pure anion to 1.374 Å in the molecule (Table 1). The vibrations at 944, 1018 cm^{-1} in spectra of the pair [EMIM][BF_4] are observed and assigned to mutual deformation of the cation ring and BF_4 moiety. The calculated vibrational spectrum of [EMIM][BF_4] with peaks in the range 730-1610 cm^{-1} (Fig. 12b) is in agreement with the experimental spectra which appear in the range of 750-1500 cm^{-1} (Umebayashi *et al.*, 2005) and 1000-1600 cm^{-1} (Heimer, Del Sesto, Meng, Wilkes & Carper, 2006). One of the most remarkable peaks in our theoretical spectrum is observed at 3150 cm^{-1} and assigned to C-H stretching, and it resembles the absolute peak around ~3000 cm^{-1} that has been recorded experimentally with the resolution of 2 cm^{-1} (Heimer *et al.*, 2006). The calculated wagging mode of C-H at 978 cm^{-1} corresponds to the experimental band 960 cm^{-1} of liquid [EMIM][BF_4] (Heimer *et al.*, 2006). Generally, our simulated vibrational modes of the [BMIM][BF_4] accord well with the major experimental peaks of liquid [BMIM][BF_4] (Umebayashi *et al.*, 2005; Heimer *et al.*, 2006).

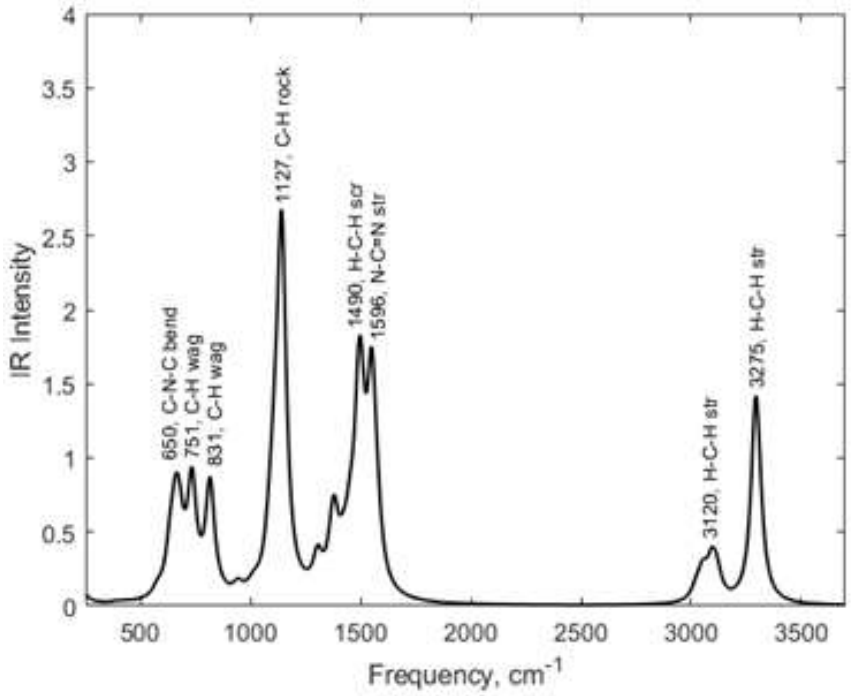
IR Intensity
Frequency, cm-1
650, C-N-C bend
751, C-H wag
831, C-H wag
1127, C-H rock
1490, H-C-H scr
1596, N-C=N str
3120, H-C-H str
3275, H-C-H str

(a)

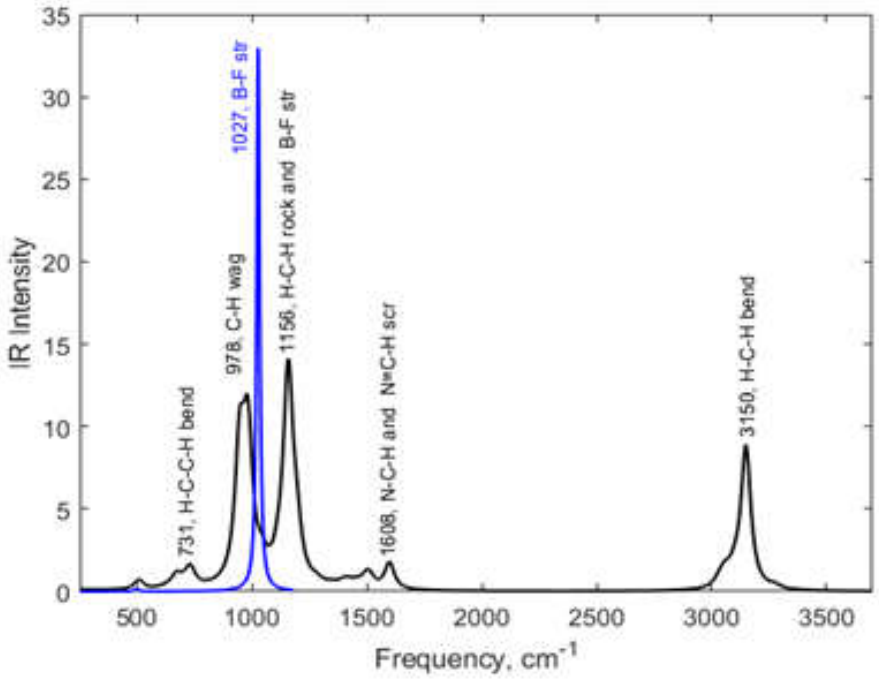
IR Intensity
Frequency, cm-1
731, H-C-C-H bend
978, C-H wag
1027, B-F str
1156, H-C-H rock and B-F str
1608, N-C-H and N=C-H scr
3150, H-C-H bend

(b)

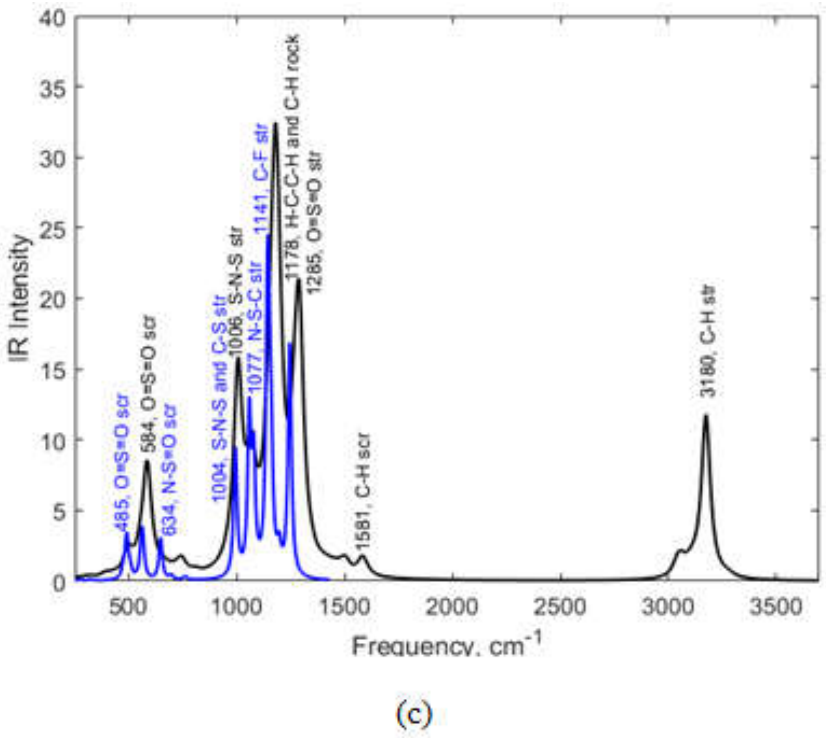

(c)

Figure 12: Calculated IR spectra of free ions and ionic pairs: (a) cation [EMIM]+; (b) anion $[BF_4]^-$ and [EMIM][BF_4]; (c) anion $[NTf_2]^-$ and [EMIM][NTf_2]. Spectra of the anions in (b) and (c) are shown in blue

The IR spectrum of the [EMIM][NTf_2] ion pair is shown in Figure 12c together with that of the anion $[NTf_2]^-$ has the following characteristics; in two regions, 500-700 and 1000-1500 cm^{-1}, overlapping of modes originated from anion and the neutral molecule is observed. The majority of modes are located in the middle-frequency region. The most intensive peak at 1178 cm^{-1} is responsible for interaction between anionic fragment and cationic part of the imidazolium ring. The band at ~1290 cm^{-1} relates to stretching S=O bonds. The intense peaks at ~1000 and ~1180 cm^{-1} correspond to the S-N-S, S=O and N-S-C stretching vibrations both in the anion and molecule spectra. In the low-frequency region, three peaks of the anion (485, 575 and 634 cm^{-1}) are merged to form broadband at 584 cm^{-1} (S-N oscillation) in the ion pair. In the high-frequency region, the vibrations of the cation part only are observed; the stretching C-H mode of the methyl group directly attached to the imidazolium ring is observed at 3180 cm^{-1}. In the low and middle-frequency regions of the [EMIM][NTf_2] ion pair spectrum, the cation vibrations are suppressed and not exhibited clearly. For the neutral ion pair [EMIM][NTf_2], the experimental IR spectrum was measured and reported in (Dhumal *et al.*, 2014; Vyas *et al.*, 2014; Kazemiabnavi *et al.*, 2016). The N-C-H rocking vibration 1169 cm^{-1} (Dhumal *et al.*, 2014), our value 1178 cm^{-1} is an agreement with the latter. From the experimental data, the stretching C-F vibration modes are observed at 1182,

1200, 1227 cm^{-1} (Dhumal *et al.*, 2014) and 1192 (Vyas *et al.*, 2014), our data 1180-1190 cm^{-1} are in agreement with the experiment. In low-frequency region, our calculated frequency 584 cm^{-1} (S-N-S bending) corresponds well to the experimental frequency 569 cm^{-1} from Dhumal (2007) and 614 cm^{-1} in Kazemiabnavi *et al.* (2016). As concerns, the higher frequency region, and the C-H stretching mode at ~ 3180 cm^{-1} accord well to the experimental data 2914-3165 cm^{-1} but the intensity of the band in the simulated spectrum looks overrated. Surprisingly that one of most intensive peak (1290 cm^{-1}) of the theoretical spectra simulated in our work as well as computed in Dhumal (2007), it has been assigned to O=S stretching mode, but, it has not been recorded and analysed from experimental data.

4.5 Thermodynamics of reactions

Interactions in the molecules [EMIM][NTf_2] and [EMIM][BF_4] were considered through inter-ionic reactions (1) and (2) between the $[EMIM]^+$ cation and $[BF_4]^-$ or $[NTf_2]^-$ anions. The energies of the reactions $\Delta_r E$ were calculated as the difference between the total energies of the products and reactants:

$$\Delta_r E = \Sigma E_{prod} - \Sigma E_{react} \quad (3)$$

In quantum chemical computations, the total energies of species correspond to temperature 0 K and normal pressure. The enthalpies of the reactions $\Delta_r H°(0)$ were obtained using the Δ_rE and zero-point vibration energies $\Delta_r\varepsilon$ as follows;

$$\Delta_r H°(0) = \Delta_r E + \Delta_r\varepsilon \quad (4)$$

$$\Delta_r\varepsilon = ½[hc(\Sigma\omega_{i\ prod} - \Sigma\omega_{i\ react})] \quad (5)$$

where h is the Plank's constant, c is the speed of light in free space, $\Sigma\omega_{i\ prod}$ and $\Sigma\omega_{i\ react}$ are the sums of the vibrational frequencies of the products and reactants, respectively.

Upon examining the effect of theoretical approach, the total energies of the species were computed with different basis sets, from the 3-21G(d,p) to 6-311++G(d,p), by using the DFT B3LYP5 and CAM-B3LYP functionals. The calculated values of $\Delta_r H°(0)$ are shown in Fig. 13. The data obtained with the extended basis sets, from 6-311G(d,p) and further, approach the values about –360 kJ mol^{-1} and –320 kJ mol^{-1} for the reactions (1) and (2), respectively; whereas for the small bases sets, 3-21G(d,p) and 6-31G(d,p), the results underrated drastically, up to ~100 kJ mol^{-1}, and look unreliable. The theoretical magnitudes as computed with the most advanced approach CAM-B3LYP/6-311++G(d,p) basis set are given in Table

3; the uncertainties are roughly estimated as spreading between values by three advanced approaches 3, 4, 5 in Fig. 13. As it is seen, the $\Delta_r H°(0)$ for the [EMIM][BF_4] is about 40 kJ mol^{-1} lower than [EMIM][NTf_2], the former ion pair is bound stronger which is due to smaller size of the anion BF_4^- and shorter inter-ionic separations. The entropies of the reactions $\Delta_r S°(T)$ also have been obtained based on the same approach and the values of $\Delta_r S°(450\ K)$ are presented in Table 3. Both values are negative and close one to another.

The thermodynamic functions, molar heat capacities $c°_p(T)$, entropies $S°(T)$, enthalpy increments $H°(T)–H°(0)$, reduced Gibbs free energies $\Phi°(T)$, are listed in Table 2. Our molar heat capacity and enthalpy increment values agree well with the thermodynamic functions of $[EMIM]^+$, $[NTf_2]^-$ and [EMIM][NTf_2] from Paulechka *et al* .(2008), the trend of enthalpy increase from 12.1 kJ mol^{-1} to 67.9 kJ mol^{-1} when the temperature changes from 298.15 K to 400 K is observed to be a drastic change, the pattern that is witnessed also in literature values (Paulechka *et al.*, 2008). This shows that enthalpy is a very sensitive parameter to intramolecular vibrations, the latter might not be detectable at lower temperatures, hence the significant changes in enthalpy values closer to room temperature might be attributed by the existence of lower frequencies that were generated and used in calculation of thermodynamic functions. Meanwhile for an individual anion of $[BF_4]^-$, the good agreement is observed between the calculated entropy values and the ones from thermodynamic database, $S°(298.15\ K)$ is 270.1 and 268.7 J mol^{-1} K^{-1} (Gurvich *et al*., 1992), respectively. Upon comparing the calculated and reported (Paulechka *et al.*, 2008) entropy values which are $S°(298.15\ K)$ 743.6 and 777.9 J mol^{-1} K^{-1} for [EMIM][NTf_2], there is occurrence of small deviation. With the small difference depicted between the calculated entropy values and the literature data, it is worth to mention that in Paulechka *et al.* (2008) the thermodynamic functions were computed based on advanced approach with internal rotations contribution.

Table 2: Thermodynamic functions of the gaseous cation, anions and neutral ion pairs

T, K	c_p, J mol^{-1} K^{-1}	S, J mol^{-1} K^{-1}	$H(T)$-$H(0)$, kJ mol^{-1}	$\Phi(T)$, J mol^{-1} K^{-1}
		$[EMIM]^+$		
298.15	133.5	378.1	24.4	296.3
300	134.2	379.0	24.6	296.8
400	174.6	423.1	40.1	322.9
450	193.8	444.8	49.3	335.2
500	211.7	466.2	59.4	347.3
600	243.3	507.6	82.2	370.6
		$[BF_4]^-$		
298.15	69.2	270.1	14.1	222.8
300	69.4	270.6	14.2	223.1
400	80.1	292.1	21.7	237.7
450	84.1	301.7	25.8	244.3
500	87.4	310.8	30.1	250.5
600	92.4	327.2	39.1	262.0
		$[NTf_2]^-$		
298.15	215.0	524.6	40.1	390.2
300	215.8	526.0	40.5	391.0
400	250.5	593.0	63.9	433.4
450	264.3	623.4	76.8	452.8
500	276.0	651.8	90.3	471.3
600	294.3	703.9	118.8	505.8
		$[EMIM][BF_4]$		
298.15	216.7	511.6	39.9	377.7
300	217.7	512.9	40.3	378.5
400	269.2	582.7	64.7	421.0
450	292.6	615.8	78.8	440.8
500	314.0	647.7	93.9	459.9
600	351.0	708.4	127.2	496.3
		$[EMIM][NTf_2]$		
298.15	362.3	743.6	66.4	520.9
300	363.8	745.9	67.1	522.3
400	439.6	861.2	107.3	592.9
450	472.8	914.9	130.2	625.7
500	502.6	966.3	154.6	657.2
600	553.0	1062.6	207.4	716.9

For the [EMIM][NTf_2], the inter-ionic reaction was studied experimentally by mass spectrometric technique (Dunaev *et al.*, 2016) and by Knudsen effusion method which has been integrated with a quartz crystal microbalance (Rocha *et al.*, 2011), partial pressures of charged species $[EMIM]^+$ and $[NTf_2]^-$ and neutral ion pair [EMIM][NTf_2] were measured at ~400-500 K and reported in Dunaev *et al.*, (2016) for charged species and in Rocha *et al.* (2011) for neutral ion pair. By using this data, we have calculated equilibrium constants of the reaction (2) and plotted $\ln K^{o}_{p}$ vs $1/T$ (Fig. 14). According to the van't Hoff equation the slope of the plot gives the enthalpy the reaction $\Delta_r H°(T) = -284.9$ kJ mol^{-1} which has been recalculated to 0 K with our enthalpy increments $H°(T) - H°(0)$; $\Delta_r H°(0) = -289.3$ kJ mol^{-1}. The range of thermodynamic functions of the charged species of $[EMIM]^+$, $[BF_4]^-$, $[NTf_2]^-$ and neutral ion pair of [EMIM][BF_4] and [EMIM][NTf_2] in the gas phase as function of temperature are listed in Appendix 3.

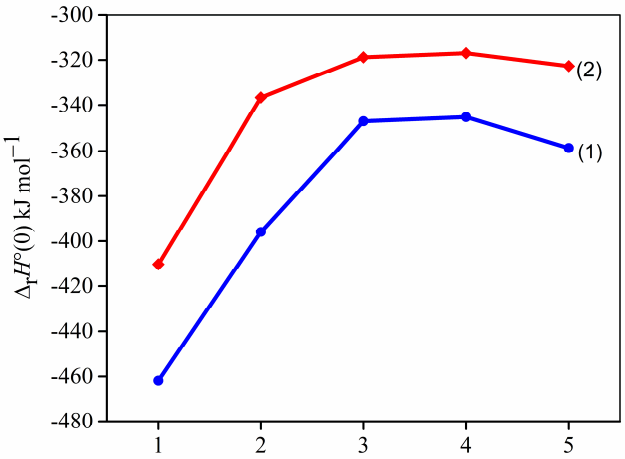

Figure 13: Enthalpies of interionic reactions (1) and (2) versus level of computation: 1 – B3LYP5/3-21G(d,p), 2 – B3LYP5/6-31G(d,p), 3 – B3LYP5/6-311G(d,p), 4 – B3LYP5/6-311++G(d,p), 5 – CAM-B3LYP5/6-311++G(d,p)

Also, the evaluation of $\Delta_r H°(0)$ based on the third law of thermodynamics has been employed:

$$\Delta_r H°(0) = T[\Delta_r \Phi°(T) - R\ln K^{o}_{p}(T)] \quad (6)$$

where $\Delta_r \Phi°(T)$ represents the reduces Gibbs free energy of the reaction at a temperature T.

The values of $\Phi°(T)$ and other thermodynamic functions required were computed using the optimised geometrical parameters and vibrational frequencies simulated at CAM-B3LYP/6-311++G(d,p) approach. The enthalpy appeared to be $\Delta_r H°(0) = -275$ kJ mol^{-1}, that differs from that based on the van't Hoff law by 14 kJ mol^{-1}. The discrepancy might be attributed

partly to the inaccuracy of experimentally measured pressures in Dunaev *et al.* (2016) and Rocha *et al.* (2011) as well as thermodynamic functions calculated. Regarding the latter, it is known that thermodynamic functions are highly sensitive to non-rigidity of the geometrical structure and that non-rigidity might be exhibited through low vibrational frequencies occurrence. For the [EMIM][NTf_2] ionic pair, low frequencies, 11, 23, 27 cm^{-1} were found in simulated spectrum with CAM-B3LYP functional, while usage of the B3LYP5 gave even lower frequencies: 3, 8, 25 cm^{-1} with the same basis set 6-311++G(d,p). That resulted in noticeably different thermodynamic properties: $\Delta_r\Phi°$(450 K) were –162.4 and –127.1 J mol^{-1} K^{-1}; $\Delta_r H°(0)$ –275.1 and –144.8 kJ mol^{-1}, as obtained with the CAM-B3LYP and B3LYP5, respectively. Among the two values of $\Delta_r H°(0)$, the first one is closer to that based on the van't Hoff equation , meanwhile a temperature trend about 6% in $\Delta_r H°(0)$ was observed for the range 400-500 K. The results of treatment of the experimental data (Rocha *et al.*, 2011; Dunaev *et al.*, 2016) are given in Table 3 and denoted "Based on expt." the uncertainties have been estimated based of statistical errors in Rocha *et al.* (2011) and Dunaev *et al.* (2016).

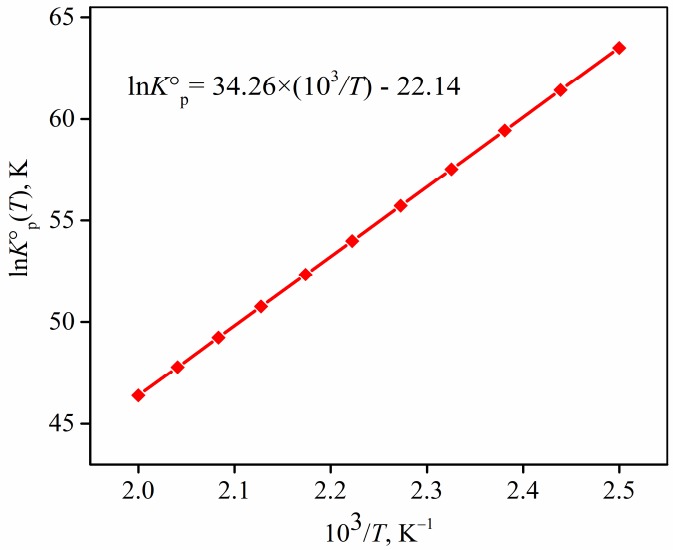

Figure 14: Temperature dependence of $\ln K_p^{\circ}(T)$ for the reaction (2)

Table 3: Thermodynamic characteristics of the reactions; all values in kJ mol^{-1}

No	Reaction	Theoretical results			Based on the expt.	
		$-\Delta_r E$	$\Delta_r\varepsilon$	$-\Delta_r H°(0)$	$-\Delta_r H°(0)$	
1	$[EMIM]^+ + [BF_4]^- = [EMIM][BF_4]$	363.8	5.2	358.7		
2	$[EMIM]^+ + [NTf_2]^- = [EMIM]\ [NTf_2]$	326.8	4.1	322.7	276.7[a]	321.2[b]

[a] Found by using Eq.(6). [b] Found by using the van't Hoff equation and enthalpy increments $H°(T)–H°(0)$ to calculate $\Delta_r H°(0) = \Delta_r H°(T) + \Delta_r[H°(T)–H°(0)]$ the value of $\Delta_r H°$(450 K) is

found directly from the slope in Fig.14. The thermodynamic functions used were obtained with CAM-B3LYP/6-311++G(d,p) method

4.6 Estimation of energy of reaction by simple ionic model

Following the nature of ionic liquids as composed of two opposite charged moieties, a simple ionic model might be suggested to estimate their interaction energy. The parameters of the hydrogen bonds, inter-nuclear separations and Mulliken atomic charges can be used in modeling as displayed in Table 4. The rough estimation gives quite reasonable energy values –376 and –346 kJ mol^{-1} for reaction (1) and (2), respectively. By considering inter-ionic reactions shown in Table 3, the energies of reactions for the two neutral ion pairs were estimated by the simple ionic model and the formula which was considered is given by:

$$E_T = \sum_{i}^{j}\left(\frac{Q_i Q_j}{4\pi\varepsilon_{\bullet} R_{ij}}\right), \text{kJ mol}^{-1} \tag{7}$$

Table 4: Total energy derived from concept of simple ionic model

Inter-atomic distance	R(i-j), Å	Mulliken charge	Q(i), C	$E_{i,j}$, kJ mol^{-1}
		[EMIM][BF_4]		
R(F3-H1)	2.702	Q(F3)	–0.446	E_1 = –76.309
R(F4-H4)	2.393	Q(F4)	–0.401	E_2 = –63.362
R(F4-H1)	2.119	Q(F2)	–0.412	E_3 = –87.486
R(F1-H1)	2.220	Q(H4)	0.274	E_4 = –85.796
R(F2-H10)	2.194	Q(H1)	0.335	E_5 = –63.231
		Q(H10)	0.244	E_T = –376.184
		[EMIM][NTf_2]		
R(O2-H4)	2.198	Q(O2)	–0.266	E1 = –51.271
R(O2-H1)	2.123	Q(H4)	0.307	E2 = –109.795
R(O4-H1)	2.114	Q(H1)	0.635	E3 = –118.553
R(O4-H10)	2.128	Q(O4)	–0.286	E4 = –66.027
		Q(H10)	0.356	ET = –345.647

4.7 Electrochemical performance of the system

The cyclic voltammetry was performed on activated carbon electrode with two ionic liquids at a scan rate ranging from 5 mV s^{-1} to 100 mV s^{-1}. Figure 1 shows cyclic voltammograms at

the scan rate of 10 and 20 mV s^{-1}, and in the potential range between –1.2 and 1.6 V. In typical capacitor, the exhibited shape of the voltammograms appears rectangular shape which is contributed by the existence of low contact resistances between the electrodes (Elgrishi *et al.*, 2017; Shabeeba, Thayyil, Pillai, Soufeena & Niveditha, 2018) but the shape of voltammograms displayed in Fig. 15(a) and (b) suffers from a loop distortion due to total resistance as the result of electrode-electrolyte interaction forming capacitive reactance, charge transfer resistance and uncompensated resistance from the electrolyte (Subramanian *et al.*, 2007).

It is the behaviour of the activated carbon to exhibit the capacitive behaviour in a region of negative potential window when integrated with aqueous electrolytes, in this study the redox properties and capacitive behaviour of activated carbon working in imidazolium ionic liquids have been displayed in both negative and positive regions of potential window (from –1.2 to 1.6 V). At a low scan rate of 5-10 mV s^{-1} for both ionic liquids, the cathodic peak was getting steeper, and the electrolyte was forming mild clouds indicating that the ions were strongly absorbed or desorbed as the chemical reaction was taking place accordingly within negative region of the applied potential (Elgrishi *et al.*, 2017).

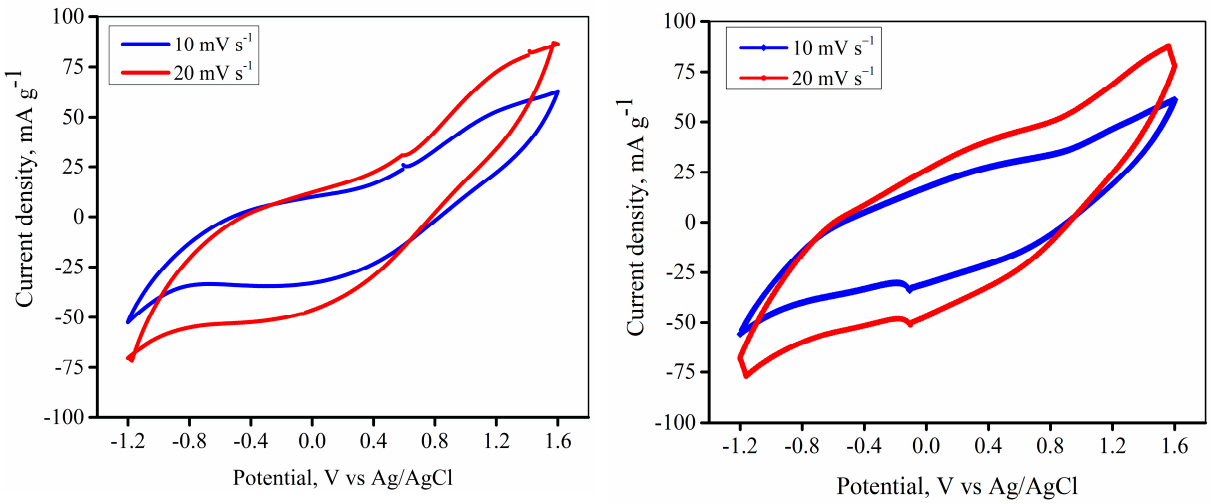

(a) (b)

Figure 15: Cyclic voltammograms of (a) AC/ $EMIMBF_4$ (b) AC/ $EMIMNTf_2$ at scanning rates of 10 and 20 mV s^{-1}

The specific capacitance shown by both imidazolium ionic liquids and activated carbon at room temperature in this work is lower compared to the value of specific capacitance reported when a cyclic voltammetry is conducted between aqueous electrolyte and activated carbon as electrode which is around 200 F g^{-1} , the smaller value in specific capacitance was

probably attributed by the small size of the pore size of the activated carbon compared to the ionic size of the ionic liquids' constituents (Rennie, Martins, Smith & Hall, 2016). In order to get the specific capacitance of the electrode, C_s, the integral areas from the voltammogram under different scan rates were estimated according to Equation 8 (Kim, Kim, Kang, Han & Roh, 2013):

$$C_s = \frac{1}{2mv(V_2 - V_1)} \int_{V1}^{V2} I(V)dV \tag{8}$$

where $\int_{V1}^{V2} I(V)dV$ is the total area defined by the absolute integral loop inscribed by the voltammogram, v is the scan rate, (V_2–V_1) is the potential window and m is the mass of electrodes.

The difference in specific capacitance for both ionic liquids seems to be very small with [EMIM][NTf_2] being higher by 2.4% (Fig. 16). The closeness of specific capacitances between the two ionic liquids might be contributed by the same properties of the cationic part (Van Aken *et al.*, 2014) compared to anions which are different, hence making the effect of different anionic parts less pronounced. Moreover, for both ionic liquids the effect of scan rates in specific capacitance is clearly shown as the specific capacitance values are gradually decreasing from around 4 to 0.4 F g^{-1} when the scan rate is applied from 5 to 100 mV s^{-1}. As the dependence of capacitance of electrochemical cell on the pore size is very intense, the small values of specific capacitances for ionic liquids might be caused by improper packing and distribution of ionic species near the pores of activated carbon (Neal, Wesolowski, Henderson & Wu, 2018).

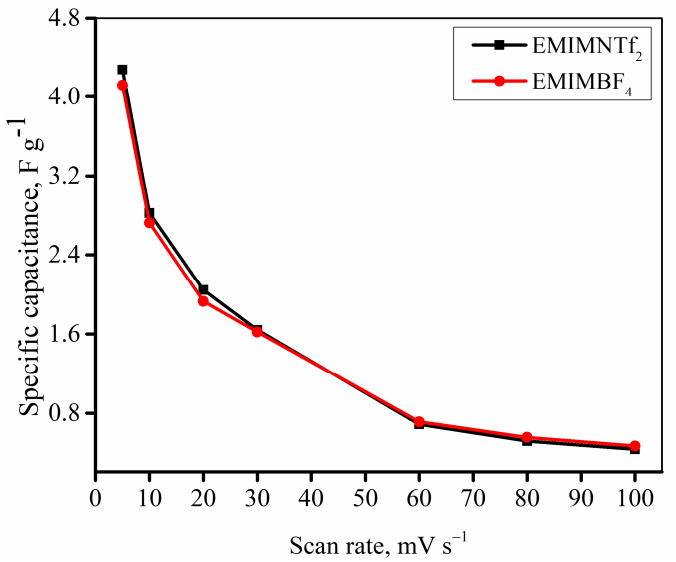

Figure 16: Specific capacitance versus scan rates in 2 M of [EMIM][BF_4] and [EMIM][NTf_2] prepared in acetonitrile

The resistivity nature of the electrochemical system was studied by employing frequency response analysis (FRA) method; the study surveys the contribution of electrode materials, nature of the electrolyte and interaction between the two active components of the electrochemical system. The data from the FRA measurements helps to analyse the capability of the electrochemical cell in storing of the electrical charges. The best representation of the data extracted from the experiment is by drawing Nyquist and Bode plots whereby the Nyquist part is presented in a complex quantity form with the imaginary part of the impedance as the function of the real impedance. Usually, the Bode plot takes the phase angle or the real impedance as the function of frequency.

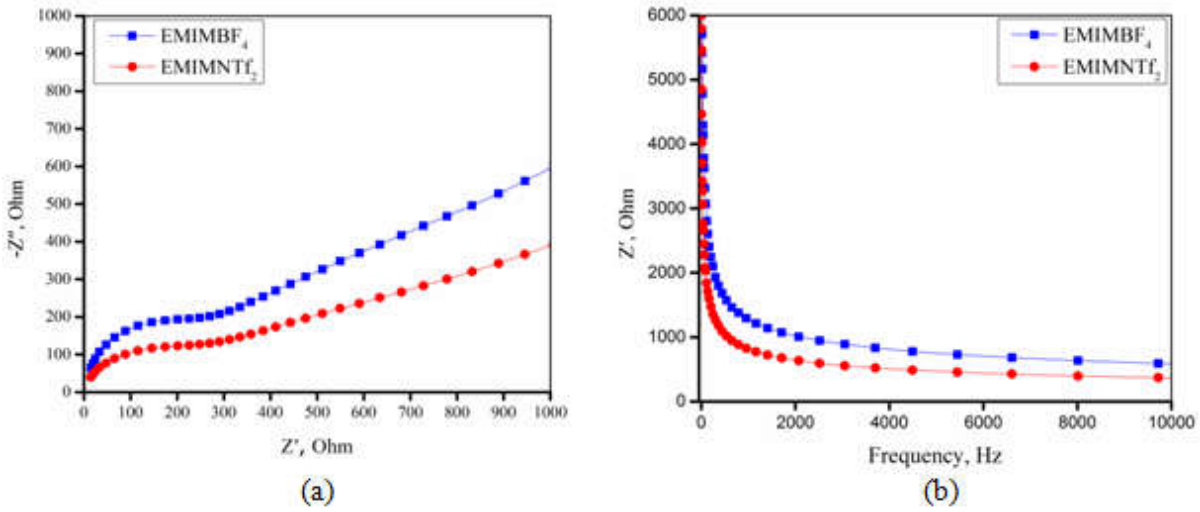

Figure 17: Nyquist plot (a) and Bode plot (b), for [EMIM][BF_4] and [EMIM][NTf_2] in 2 M concentration prepared in acetonitrile

From the Fig. 17 (a) the shape of the electrochemical semicircle, which characterises the simplified equivalent electrical circuit was analysed with the electrolyte resistance of approximately 3.8 Ohms and 2.9 Ohms for [EMIM][BF_4] and [EMIM][NTf_2] respectively. At the high-frequency region, the polarisation resistance is characterised by the diameter of the semicircles, which corresponds to the magnitude of the charge transfer resistance. The increased resistance in [EMIM][NTf_2] might have been contributed by low diffusion coefficient of the [EMIM][NTf_2] which also might be attributed by its molecular size (Vu *et al.*, 2013; Van Aken *et al.*, 2014; Rennie *et al.*, 2016). The Bode plot displayed in Fig. 17 (b) reveals that at low frequency, the high impedance dominates with [EMIM][NTf_2] being at lower resistance compared to [EMIM][BF_4] which intersects with a vertical axis at high impedance values.

Using cyclic voltammetry and electrochemical impedance spectroscopy method, the interaction between activated carbon and imidazolium-based ionic liquids as electrolyte was studied., a potential window of 2.8 V which was set for both ionic liquids resulted into achieving the specific capacitances of 4.1 F g^{-1} and 4.3 F g^{-1} for [EMIM][BF_4] and [EMIM][NTf_2] respectively, at the lower scan rate of 5 mV s^{-1}. The maximum current density reached during scanning process was 87 mA g^{-1} and 88 mA g^{-1} for [EMIM][BF_4] and [EMIM][NTf_2] respectively. Both ionic liquids exhibited the electrochemical semicircles within the frequency range of 0.01 Hz to 1 MHz after setting 100 numbers of frequencies in FRA, the behaviour which represents the resistive and capacitive nature of the

electrochemical system and the equivalent circuit components being aligned in a parallel arrangement.

4.8 Energy density and power density for both IILs

It can be evidently seen that [EMIM][BF_4] in electrochemical system delivered specific energy and specific power higher than [EMIM][NTf_2]. The trend shows that at high scan rate for both electrolytes the energy density is nine times lower than the value obtained at low scan rate, signifying that at low scan rate more charges are stored on surface of electrode rendering to high specific capacitance, a unique property for calculation of energy density. The superiority of our electrochemical system was substantiated by comparing the energy density and power density of with existing literature data (Jiang, 2017), and it can be visualised that at both scan rate the power densities for both electrolytes were superior to literature data as shown in Table 5. The energy density and power density were calculated based on the following equations:

$$E = 1/2\, CV^2 \tag{9}$$

$$P = VI_s \tag{10}$$

where E stands for energy density of the system (Wh kg^{-1}), C is the specific capacitance (F g^{-1}), V is the operating voltage window (V), P is the power density (W kg^{-1})and I_s is the current density (A g^{-1}).

Table 5: Comparison of energy density and power density for both IILs

Scan rate, mV s^{-1}	[EMIM][BF_4]		[EMIM][NTf_2]		[BMIM][BF_4][c]	
	Energy density, Wh kg^{-1}	Power density, W kg^{-1}	Energy density, Wh kg^{-1}	Power density, W kg^{-1}	Energy density, Wh kg^{-1}	Power density, W kg^{-1}
5	4.48	160	4.66	120	6.6	20
100	0.51	264	0.48	244	3.3	200

[c](Jiang, 2017)

4.9 Conventional charge-discharge of the supercapacitor prototype

The charging-discharging of supercapacitor prototype was carried out by using conventional method, whereby the maximum voltage of 9 V was applied to its terminals and the discharging process was performed by connecting a load (LED) to its terminal. The trend of

charging and discharging behaviour was recorded after the every 10 seconds, and the graphs were drawn as shown in Fig. 18.

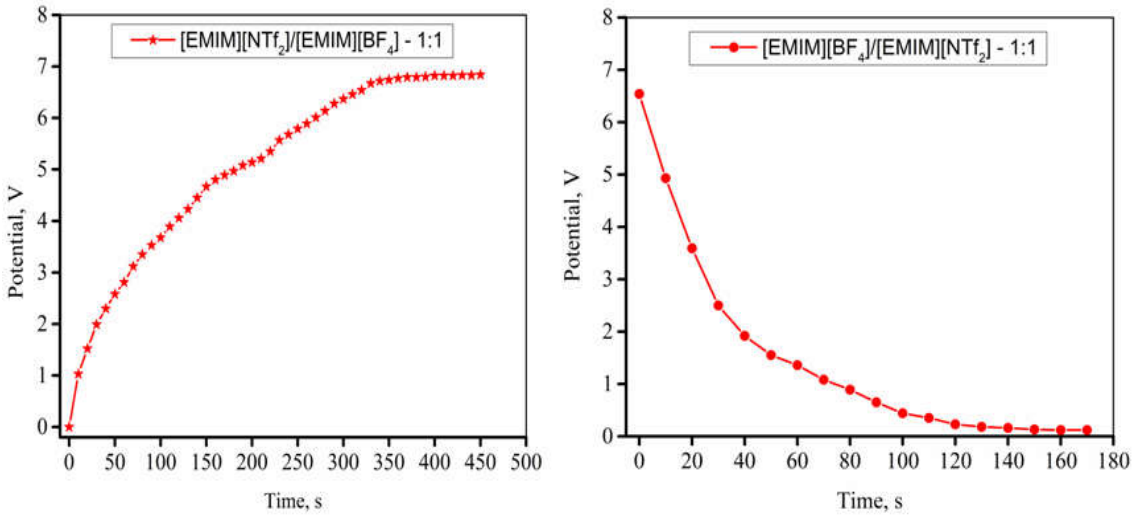

(a) (b)

Figure 18: Charging and discharging curves of the supercapacitor prototype

The charging and discharging of the supercapacitor prototype were done under the time interval of ten seconds; the prototype exhibited the capacitive behaviour whereby the voltage varied exponentially with the time elapse during charging and discharging process. During charging process, the voltage reached 76% of its initial voltage of 9 V this shows that the saturation of AC electrodes saturate faster when interact with imidazolium based ionic liquids at room temperature, the counter-effect which might be contributed by the bigger size of ions compared to mesopores and micropores present in electrode materials. The discharging decreases at high rate compared to charging process, the process starts with 95.6% of its initial voltage after being full charged. The loss of 4.4% of potential from the charged supercapacitor happens due to self discharging effect shown by the prototype, with the load of 1000 Ohms, the supercapacitor has been capable to empty the voltage for 170 seconds.

CHAPTER FIVE

CONCLUSION AND RECOMMENDATIONS

5.1 Conclusion

The following conclusions could be drawn based on the findings obtained in this research:

(i) The interaction between the $[EMIM]^+$ cation and two anions, $[BF_4]^-$ and $[NTf_2]^-$ which resulted in ion pairs $[EMIM][BF_4]$ and $[EMIM][NTf_2]$ formation, was investigated from where the ion pairs have been coupled by the Coulombic forces and hydrogen bonding. The energies and enthalpies of the reactions were determined.

(ii) The frontier molecular orbitals have been analysed; in both ion pairs the electron density in HOMO is concentrated in the anionic moieties, while that of LUMO is located in the cationic part. It is interesting that the HOMO energies difference between ion pair and respective anion practically coincides with the enthalpy of the association reaction. It appeared that lowering of the HOMOs energies in the neutral pairs compared to free anions occurred due to the cation-anion coupling.

(iii) The study on the effect of interaction between the neighbor atoms linked by hydrogen bonding revealed that there is possibility of predicting reasonable energy of inter-ionic reactions by simple ionic model.

(iv) Experimental study of imidazolium-based ionic liquids was attempted through electrochemical techniques whereby the cyclic voltammetry produced the electrochemical parameters of electrode-electrolyte interaction are mostly dependent on the electrochemical window of electrolyte.

(v) The closeness in electrochemical properties like specific capacitances and energy densities for both electrolytes revealed that existence of anions of $[BF_4]$ and $[NTf_2]$ in imidazolium based ionic liquids has little influence over the cation [EMIM] in altering the chemical properties.

(vi) The frequency response analysis helped to investigate the impedance of electrode-electrolyte interaction and both electrolytes together with AC carbon electrode in the

high frequency region displayed semi-circles, an indicator for the charge transfer resistance. The results of both imidazolium-based ionic liquids confirm that the displayed electrochemical potential window is an influential factor for raising the energy density of the electrochemical cells.

5.2 Recommendations

Based on the potentiality of the energy storage devices, the practical electrochemical system is proposed to be enhanced with some factors that the future work should take into consideration; therefore, the following recommendations are to be observed:

(i) The electrochemical system was carried out in room temperature where the ionic mobility of room temperature ionic liquids is limited; there is a need to perform the experiment at high temperature for optimization of capacitance through ionic mobility as the ILs themselves are thermally stable up to 350 °C.

(ii) The pore size of the electrode materials seems to be not compatible with the size of the ILs, limiting the adsorption process for ions to be stored in a good number. The future work should consider the electrode materials with large pore size in order to accumulate more charges for high capacitance.

(iii) Direct determination of charge-discharge behaviour of the supercapacitor prototype was not achieved due to low current supplied by the PGSTAT204 (Metrohm Autolab - AUT 50663) machine, It is recommended that for effective examination of energy density and power density of electrochemical system, the potentiostat-galvanostat machine with the capability to supply high current should be used in parallel with a probe of two-cell setup.

(iv) Further electrochemical characterization of imidazolium based ionic liquids should be done in different concentrations in order to investigate their effects on capacitance of the energy storage system.

REFERENCES

Andres, B., Forsberg, S., Vilches, A. P., Zhang, R., Hummelgård, M., Bäckström, J., . . . Andersson, H. (2012). Supercapacitors with graphene coated paper electrodes. *Nordic Pulp & Paper Research Journal*, *27*(2), 481-485. doi: 10.3183/npprj-2012-27-02-p481-485.

Balducci, A. (2016). Electrolytes for high voltage electrochemical double layer capacitors: A perspective article. *Journal of Power Sources*, *326,* 534-540. doi: 10.1016/j.jpowsour.2016.05.029.

Balducci, A., Dugas, R., Taberna, P., Simon, P., Plee, D., Mastragostino, M., & Passerini, S. (2007). High temperature carbon–carbon supercapacitor using ionic liquid as electrolyte. *Journal of Power Sources*, *165*(2), 922-927. doi: 10.1016/j.jpowsour.2006.12.048.

Bard, A. J., Abruna, H. D., Chidsey, C. E., Faulkner, L. R., Feldberg, S. W., Itaya, K., . . . Murray, R. W. (1993). The electrode/electrolyte interface-a status report. *The Journal of Physical Chemistry*, *97*(28), 7147-7173. doi: 10.1021/j100130a007.

Bleda-Martínez, M. J., Maciá-Agulló, J. A., Lozano-Castelló, D., Morallon, E., Cazorla-Amorós, D., & Linares-Solano, A. (2005). Role of surface chemistry on electric double layer capacitance of carbon materials. *Carbon*, *43*(13), 2677-2684. doi: 10.1016/j.carbon.2005.05.027.

Bode, B. M., & Gordon, M. S. (1998). MacMolPlt. Version 7.4.2. *Journal of Molecular Graphics and Modelling*, *16*(3), 133-138 doi: 10.4236/oalib.1101978.

Chiappe, C., & Pieraccini, D. (2005). Ionic liquids: solvent properties and organic reactivity. *Journal of Physical Organic Chemistry*, *18*(4), 275-297. doi: 10.1002/poc.863.

Cho, C., Preiss, U., Jungnickel, C., Stolte, S., Arning, J. r., Ranke, J., . . . Thöming, J. (2011). Ionic liquids: predictions of physicochemical properties with experimental and/or DFT-calculated LFER parameters to understand molecular interactions in solution. *The Journal of Physical Chemistry B*, *115*(19), 6040-6050. doi: 10.1021/jp200042f.

Choi, H., Jung, S.-M., Seo, J., Chang, D. W., Dai, L., & Baek, J. (2012). Graphene for energy conversion and storage in fuel cells and supercapacitors. *Nano Energy*, *1*(4), 534-551. doi: 10.1016/j.nanoen.2012.05.001.

Danielewicz, D., Kmiotek, M., & Surma-Ślusarska, B. (2019). Study of ionic liquids UV-VIS and FTIR spectra before and after heating and spruce groundwood dissolution. *Fibres and Textiles in Eastern Europe*, *27*(1), 118-123. doi: 10.5604/01.3001.0012.7515.

Deng, J., Lu, X., Liu, L., Zhang, L., & Schmidt, O. G. (2016). Introducing Rolled-Up Nanotechnology for Advanced Energy Storage Devices. *Advanced Energy Materials*, *6*(23), 1600797. doi: 10.1002/aenm.201600797.

Dhumal, N. R. (2007). Molecular interactions in 1, 3-dimethylimidazolium-bis (trifluromethanesulfonyl) imide ionic liquid. *Chemical Physics*, *342*(1-3), 245-252. doi: 10.1016/j.chemphys.2007.10.004.

Dhumal, N. R., Noack, K., Kiefer, J., & Kim, H. J. (2014). Molecular structure and interactions in the ionic liquid 1-ethyl-3-methylimidazolium bis (trifluoromethylsulfonyl) imide. *The Journal of Physical Chemistry A*, *118*(13), 2547-2557. doi: 10.1021/jp502124y.

Dong, K., Liu, X., Dong, H., Zhang, X., & Zhang, S. (2017). Multiscale studies on ionic liquids. *Chemical Reviews*, *117*(10), 6636-6695. doi: 10.1021/acs.chemrev.6b00776.

Dunaev, A. M., Motalov, V. B., Kudin, L. S., & Butman, M. F. (2016). Molecular and ionic composition of saturated vapor over $EMImNTf_2$ ionic liquid. *Journal of Molecular Liquids*, *219*, 599-601. doi: 10.1016/j.molliq.2016.03.074.

Dyatkin, B., Osti, N. C., Zhang, Y., Wang, H. W., Mamontov, E., Heller, W. T., . . . Wesolowski, D. J. (2018). Ionic liquid structure, dynamics, and electrosorption in carbon electrodes with bimodal pores and heterogeneous surfaces. *Carbon*, *129*, 104-118. doi: 10.1016/j.carbon.2017.12.001.

Eftekhari, A. (2018). The mechanism of ultrafast supercapacitors. *Journal of Materials Chemistry A*, *6*(7), 2866-2876. doi: 10.1039/C7TA10013B.

Eftekhari, A., & Saito, T. (2017). Synthesis and properties of polymerized ionic liquids. *European Polymer Journal 90*, 245-272. doi: 10.1016/j.eurpolymj.2017.03.033.

Elgrishi, N., Rountree, K. J., McCarthy, B. D., Rountree, E. S., Eisenhart, T. T., & Dempsey, J. L. (2017). A practical beginner's guide to cyclic voltammetry. *Journal of Chemical Education*, *95*(2), 197-206. doi: 10.1021/acs.jchemed.7b00361.

Eshetu, G. G., Armand, M., Ohno, H., Scrosati, B., & Passerini, S. (2016). Ionic liquids as tailored media for the synthesis and processing of energy conversion materials. *Energy & Environmental Science*, *9*(1), 49-61. doi: 10.1039/C5EE02284C.

Fic, K., Meller, M., Menzel, J., & Frackowiak, E. (2016). Around the thermodynamic limitations of supercapacitors operating in aqueous electrolytes. *Electrochimica Acta*, *206*, 496-503. doi: 10.1016/j.electacta.2016.02.077.

Forse, A. C., Merlet, C. l., Griffin, J. M., & Grey, C. P. (2016). New perspectives on the charging mechanisms of supercapacitors. *Journal of the American Chemical Society*, *138*(18), 5731-5744. doi: 10.1021/jacs.6b02115.

Frackowiak, E. (2007). Carbon materials for supercapacitor application. *Physical Chemistry Chemical Physics*, *9*(15), 1774-1785. doi: 10.1039/B618139M.

Frackowiak, E., & Beguin, F. (2001). Carbon materials for the electrochemical storage of energy in capacitors. *Carbon*, *39*(6), 937-950. doi: 10.1016/S0008-6223(00)00183-4.

Godillot, G., Taberna, P. L., Daffos, B., Simon, P., Delmas, C., & Guerlou-Demourgues, L. (2016). High power density aqueous hybrid supercapacitor combining activated carbon and highly conductive spinel cobalt oxide. *Journal of Power Sources*, *331*, 277-284. doi: 10.1016/j.jpowsour.2016.09.035.

Granovsky, A. A. (1994-2018). GAMESS Package Firefly 8.2.0. Retrieved from http://classic.chem.msu.su/gran/firefly/index.html.

Groom, C. R., Bruno, I. J., Lightfoot, M. P., & Ward, S. C. (2016). The Cambridge structural database. *Acta Crystallographica Section B: Structural Science, Crystal Engineering and Materials*, *72*(2), 171-179. doi: 10.1107/S2052520616003954.

Gurvich, L. V., Yungman, V. S., Bergman, G. A., Veitz, I. V., Gusarov, A. V., Iorish, V. S., . . . Aristova, N. M. (1992). Thermodynamic properties of individual substances. Ivtanthermo for windows database on thermodynamic properties of individual substances and thermodynamic modeling software. 3.0 Retrieved from https:// www.sciencedirect.com/science/article/abs/pii/S0364591699000231.

Hassibi, A., Navid, R., Dutton, R. W., & Lee, T. H. (2004). Comprehensive study of noise processes in electrode electrolyte interfaces. *Journal of Applied Physics*, *96*(2), 1074-1082. doi: 10.1063/1.1755429.

He, Z., & Alexandridis, P. (2015). Nanoparticles in ionic liquids: interactions and organization. *Physical Chemistry Chemical Physics 17*(28), 18238-18261. doi: 10.1039/C5CP01620G.

Heimer, N. E., Del Sesto, R. E., Meng, Z., Wilkes, J. S., & Carper, W. R. (2006). Vibrational spectra of imidazolium tetrafluoroborate ionic liquids. *Journal of Molecular Liquids*, *124*(1-3), 84-95. doi: 10.1016/j.molliq.2005.08.004.

Hu, Z., & Srinivasan, M. (2001). Mesoporous high-surface-area activated carbon. *Microporous and Mesoporous Materials*, *43*(3), 267-275. doi: 10.1016/S1387-1811(00)00355-3.

Huggins, R. A. (2000). Supercapacitors and electrochemical pulse sources. *Solid State Ionics*, *134*(1-2), 179-195. doi: 10.1016/S0167-2738(00)00725-6.

Hunt, P. A., Gould, I. R., & Kirchner, B. (2007). The structure of imidazolium-based ionic liquids: Insights from ion-pair interactions. *Australian Journal of Chemistry*, *60*(1), 9-14. doi: 10.1071/CH06301.

Janesko, B. G. (2011). Modeling interactions between lignocellulose and ionic liquids using DFT-D. *Physical Chemistry Chemical Physics*, *13*(23), 11393-11401. doi: 10. 1039/C1CP20072K.

Jiang, D., Meng, D., & Wu, J. (2011). Density functional theory for differential capacitance of planar electric double layers in ionic liquids. *Chemical Physics Letters*, *504*(4-6), 153-158. doi: 10.1016/j.cplett.2011.01.072.

Jiang, H., Lee, P. S., & Li, C. (2013). 3D carbon based nanostructures for advanced supercapacitors. *Energy & Environmental Science*, *6*(1), 41-53. doi: 10. 1039/C2EE23284G.

Jiang, J. (2017). High temperature monolithic biochar supercapacitor using ionic liquid electrolyte. *Journal of The Electrochemical Society*, *164*(8), H5043-H5048. doi: 10.1149/2.0211708jes.

Jiang, L., Wang, Z., Geng, D., Lin, Y., Wang, Y., An, J., . . . Zhang, Z. (2015). Structure and electromagnetic properties of both regular and defective onion-like carbon nanoparticles. *Carbon*, *95*, 910-918. doi: 10.1016/j.carbon.2015.09.016.

Jiang, W., Hu, F., Yan, Q., & Wu, X. (2017). Investigation on electrochemical behaviors of $NiCo_2O_4$ battery-type supercapacitor electrodes: the role of an aqueous electrolyte. *Inorganic Chemistry Frontiers*, *4*(10), 1642-1648. doi: 10.1039/C7QI00391A.

Johns, P. A., Roberts, M. R., Wakizaka, Y., Sanders, J. H., & Owen, J. R. (2009). How the electrolyte limits fast discharge in nanostructured batteries and supercapacitors. *Electrochemistry Communications*, *11*(11), 2089-2092. doi: 10.1016/j.elecom.2009. 09.001.

Kar, M., Plechkova, N. V., Seddon, K. R., Pringle, J. M., & MacFarlane, D. R. (2019). Ionic liquids–further progress on the fundamental issues. *Australian Journal of Chemistry*, *72*(2), 3-10. doi: 10.1071/CH18541.

Karnan, M., Subramani, K., Srividhya, P., & Sathish, M. (2017). Electrochemical studies on corncob derived activated porous carbon for supercapacitors application in aqueous and non-aqueous electrolytes. *Electrochimica Acta*, *228*, 586-596. doi: 10.1016/j. electacta.2017.01.095.

Katsyuba, S. A., Dyson, P. J., Vandyukova, E. E., Chernova, A. V., & Vidiš, A. (2004). Molecular structure, vibrational spectra, and hydrogen bonding of the ionic liquid 1-ethyl-3-methyl-1H-imidazolium tetrafluoroborate. *Helvetica Chimica Acta*, *87*(10), 2556-2565. doi: 10.1002/hlca.200490228.

Katsyuba, S. A., Griaznova, T. P., Vidis, A., & Dyson, P. J. (2009). Structural studies of the ionic liquid 1-ethyl-3-methylimidazolium tetrafluoroborate in dichloromethane using

a combined DFT-NMR spectroscopic approach. *Journal Physical Chemistry B 113*(15), 5046–5051. doi: 10.1021/jp8083327.

Kazemiabnavi, S., Zhang, Z., Thornton, K., & Banerjee, S. (2016). Electrochemical stability window of imidazolium-based ionic liquids as electrolytes for lithium batteries. *Journal Physical Chemistry B 120*(25), 5691-5702. doi: 10.1021/acs.jpcb.6b03433.

Khan, I., Saeed, K., & Khan, I. (2017). Nanoparticles: Properties, applications and toxicities. *Arabian Journal of Chemistry*, doi: 10.1016/j.arabjc.2017.05.011.

Kim, M. H., Kim, K. B., Kang, K., Han, J. T., & Roh, K. C. (2013). Ribbon-like activated carbon with a multi-structure for supercapacitors. *Journal of Materials Chemistry A*, *1*(44), 14008–14012. doi: 10.1039/C3TA13138F.

Kondrat, S., & Kornyshev, A. A. (2016). Pressing a spring: what does it take to maximize the energy storage in nanoporous supercapacitors? *Nanoscale Horizons*, *1*(1), 45-52. doi: 10.1039/C5NH00004A.

Laheäär, A., Przygocki, P., Abbas, Q., & Béguin, F. (2015). Appropriate methods for evaluating the efficiency and capacitive behavior of different types of supercapacitors. *Electrochemistry Communications*, *60*, 21-25. doi: 10.1016/j.elecom.2015.07.022.

Largeot, C., Portet, C., Chmiola, J., Taberna, P. L., Gogotsi, Y., & Simon, P. (2008). Relation between the ion size and pore size for an electric double-layer capacitor. *Journal of the American Chemical Society*, *130*(9), 2730-2731. doi: 10.1021/ja7106178.

Li, B., Dai, F., Xiao, Q., Yang, L., Shen, J., Zhang, C., & Cai, M. (2016). Nitrogen-doped activated carbon for a high energy hybrid supercapacitor. *Energy & Environmental Science*, *9*(1), 102-106. doi: 10.1039/C5EE03149D.

Lian, C., Liu, K., Van Aken, K. L., Gogotsi, Y., Wesolowski, D. J., Liu, H., . . . Wu, J. (2016). Enhancing the capacitive performance of electric double-layer capacitors with ionic liquid mixtures. *ACS Energy Letters*, *1*(1), 21-26.

Libich, J., Máca, J., Vondrák, J., Čech, O., & Sedlaříková, M. (2018). Supercapacitors: Properties and applications. *Journal of Energy Storage*, *17*, 224-227. doi: 0.1016/j. est.2018.03.012.

Lin, R. (2012). Formulation of electrolytes based on ionic liquids for supercapacitor applications (Doctoral Degree Thesis for the Award of Université de Toulouse, l'université Toulouse III – Paul Sabatier). Retrieved from http://thesesups.ups-tlse.fr/1895/1/2012TOU30274.pdf.

Lin, R., Taberna, P. L., Fantini, S., Presser, V., Pérez, C. R., Malbosc, F., . . . Simon, P. (2011). Capacitive Energy Storage from −50 to 100 °C Using an Ionic Liquid Electrolyte. *The Journal of Physical Chemistry Letters*, *2*(19), 2396-2401. doi: 10.1021/jz201065t.

Lin, Z., Goikolea, E., Balducci, A., Naoi, K., Taberna, P. L., Salanne, M., . . . Simon, P. (2018). Materials for supercapacitors: When Li-ion battery power is not enough. *Materials Today*, *21*(4), 419-436. doi: 10.1016/j.mattod.2018.01.035.

Liu, H., Sale, K. L., Holmes, B. M., Simmons, B. A., & Singh, S. (2010). Understanding the interactions of cellulose with ionic liquids: a molecular dynamics study. *The Journal of Physical Chemistry B*, *114*(12), 4293-4301. doi: 10.1021/jp9117437.

Liu, J., Kopold, P., van Aken, P. A., Maier, J., & Yu, Y. (2015). Energy storage materials from nature through nanotechnology: a sustainable route from reed plants to a silicon anode for lithium-ion batteries. *Angewandte Chemie International Edition*, *54*(33), 9632-9636.

Low, K., Tan, S., & Pas, E. I. (2019). An ab initio study of the structure and energetics of hydrogen bonding in ionic liquids. *Frontiers in Chemistry 7*, 208. doi: 10.3389/fchem.2019.00208.

Lu, J., Chen, Z., Ma, Z., Pan, F., Curtiss, L. A., & Amine, K. (2016). The role of nanotechnology in the development of battery materials for electric vehicles. *Nature Nanotechnology*, *11*(12), 1031. doi: 10.1038/nnano.2016.207.

MacFarlane, D., Forsyth, M., Howlett, P. C., Kar, M., Passerini, S., Pringle, J. M., . . . Zheng, W. (2016). Ionic liquids and their solid-state analogues as materials for energy generation and storage. *Nature Reviews Materials*, *1*(2), 15005. doi: 10.1038/natrevmats.2015.5.

MacFarlane, D. R., Tachikawa, N., Forsyth, M., Pringle, J. M., Howlett, P. C., Elliott, G. D., . . . Angell, C. A. (2014). Energy applications of ionic liquids. *Energy & Environmental Science*, *7*(1), 232-250. doi: 10.1039/c3ee42099j.

Maiti, S., Pramanik, A., & Mahanty, S. (2015). Influence of imidazolium-based ionic liquid electrolytes on the performance of nano-structured MnO_2 hollow spheres as electrochemical supercapacitor. *RSC Advances*, *5*(52), 41617-41626. doi: 10.1039/ C5RA05514H.

Martins, V. L., & Torresi, R. M. (2018). Ionic liquids in electrochemical energy storage. *Current Opinion in Electrochemistry*, *9*, 26-32. doi: 10.1002/celc.201701164.

Matsumoto, K., Hagiwara, R., Mazej, Z., Benkič, P., & Žemva, B. (2006). Crystal structures of frozen room temperature ionic liquids, 1-ethyl-3-methylimidazolium tetrafluoroborate ($EMImBF_4$), hexafluoroniobate ($EMImNbF_6$) and hexafluorotantalate ($EMImTaF_6$), determined by low-temperature X-ray diffraction. *solid state sciences*, *8*(10), 1250-1257. doi: 10.1016/j.solidstatesciences.2005.12.018.

McCreery, R. L. (2008). Advanced carbon electrode materials for molecular electrochemistry. *Chemical Reviews*, *108*(7), 2646-2687. doi: 10.1021/cr068076m.

Meredith, A. (2012). ChemSpider: The Free Chemical Database. Retrieved from https://doi.org/10.1108/09504121211271059.

Merlet, C., Rotenberg, B., Madden, P. A., Taberna, P. L., Simon, P., Gogotsi, Y., & Salanne, M. (2012). On the molecular origin of supercapacitance in nanoporous carbon electrodes. *Nature Materials*, *11*(4), 306. doi: 10.1038/nmat3260.

Miller, E. E., Hua, Y., & Tezel, F. H. (2018). Materials for energy storage: Review of electrode materials and methods of increasing capacitance for supercapacitors. *Journal of Energy Storage*, *20*, 30-40. doi: 10.1016/j.est.2018.08.009.

Mousavi, M. P., Wilson, B. E., Kashefolgheta, S., Anderson, E. L., He, S., Buhlmann, P., & Stein, A. (2016). Ionic liquids as electrolytes for electrochemical double-layer capacitors: Structures that optimize specific energy. *ACS Applied Materials & Interfaces*, *8*(5), 3396-3406. doi: 10.1021/acsami.5b11353.

Neal, J. N., Wesolowski, D. J., Henderson, D., & Wu, J. (2018). Electric double layer capacitance for ionic liquids in nanoporous electrodes: Effects of pore size and ion composition. *Journal of Molecular Liquids*, *270*, 145-150. doi: 10.1016/j.molliq. 2017.10.128.

Neese, F. (2012). The ORCA program system. *WIREs Computational Molecular Science 2*(1), 73-78. doi: 10.1002/wcms.81.

Ni, J., & Li, Y. (2016). Carbon nanomaterials in different dimensions for electrochemical energy storage. *Advanced Energy Materials*, *6*(17), 1600278. doi: 10.1002/aenm. 201600278.

Ong, S. P., Andreussi, O., Wu, Y., Marzari, N., & Ceder, G. (2011). Electrochemical windows of room-temperature ionic liquids from molecular dynamics and density functional theory calculations. *Chemistry of Materials*, *23*(11), 2979-2986. doi: 10. 1021/cm200679y.

Pal, P., & Ghosh, A. (2018). Solid-state gel polymer electrolytes based on ionic liquids containing imidazolium cations and tetrafluoroborate anions for electrochemical double layer capacitors: Influence of cations size and viscosity of ionic liquids. *Journal of Power Sources*, *406*, 128-140. doi: 10.1016/j.jpowsour.2018.10.051.

Pandolfo, A., & Hollenkamp, A. (2006). Carbon properties and their role in supercapacitors. *Journal of Power Sources*, *157*(1), 11-27. doi: 10.1016/j.jpowsour.2006.02.065.

Paulechka, Y. U., Kabo, G. J., Blokhin, A. V., Shaplov, A. S., Lozinskaya, E. I., Golovanov, D. G., . . . Vygodskii, Y. S. (2009). IR and X-ray study of polymorphism in 1-alkyl-3-methylimidazolium bis(trifluoromethanesulfonyl)imides. *The Journal of Physical Chemistry B*, *113*(28), 9538–9546. doi: 10.1021/jp903702c.

Paulechka, Y. U., Kabo, G. J., & Emel'yanenko, V. N. (2008). Structure, conformations, vibrations, and ideal-gas properties of 1-alkyl-3-methylimidazolium bis (trifluoromethylsulfonyl) imide ionic pairs and constituent ions. *The Journal of Physical Chemistry B*, *112*(49), 15708-15717. doi: 10.1021/jp804607n.

Pilathottathil, S., Thasneema, K., Thayyil, M. S., Pillai, M., & Niveditha, C. (2017). A high voltage supercapacitor based on ionic liquid with an activated carbon electrode. *Materials Research Express*, *4*(7), 075503. doi: 10.1088/2053-1591/aa7116.

Ray, P., Elfgen, R., & Kirchner, B. (2019). Cation influence on heterocyclic ammonium ionic liquids: a molecular dynamics study. *Physical Chemistry Chemical Physics*, *21*(8), 4472-4486. doi: 10.1039/C8CP07683A.

Rocha, M. A., Lima, C. F., Gomes, L. R., Schröder, B., Coutinho, J. A., Marrucho, I. M., . . . Lopes, J. N. C. (2011). High-accuracy vapor pressure data of the extended [C n C1im][Ntf2] ionic liquid series: trend changes and structural shifts. *The Journal of Physical Chemistry B*, *115*(37), 10919-10926. doi: 10.1021/jp2049316.

Rogers, R. D., & Seddon, K. R. (2003). Ionic liquids--solvents of the future? *Science*, *302*(5646), 792-793. doi: 10.1126/science.1090313.

Ruiz, V., Huynh, T., Sivakkumar, S. R., & Pandolfo, A. (2012). Ionic liquid–solvent mixtures as supercapacitor electrolytes for extreme temperature operation. *RSC Advances*, *2*(13), 5591-5598. doi: 0.1039/C2RA20177A.

Salanne, M. (2017). Ionic liquids for supercapacitor applications. *Topics in Current Chemistry*, *375*(3), 63. doi: 10.1007/s41061-017-0150-7.

Salanne, M., Rotenberg, B., Naoi, K., Kaneko, K., Taberna, P. L., Grey, C. P., . . . Simon, P. (2016). Efficient storage mechanisms for building better supercapacitors. *Nature Energy*, *1*(6), 16070. doi: 10.1038/nenergy.2016.70.

Schmidt, M. W., Baldridge, K. K., Boatz, J. A., Elbert, S. T., Gordon, M. S., Jensen, J. H., . . . Su, S. (1993). General atomic and molecular electronic structure system. *Journal of Computational Chemistry*, *14*(11), 1347-1363. doi: 10.1002/jcc.540141112.

Shabeeba, P., Thayyil, M. S., Pillai, M., Soufeena, P., & Niveditha, C. (2018). Electrochemical Investigation of Activated Carbon Electrode Supercapacitors. *Russian Journal of Electrochemistry*, *54*(3), 302-308. doi: 10.1134/S10231935. 17120096.

Shen, C., Wang, X., Zhang, W., & Kang, F. (2011). A high-performance three-dimensional micro supercapacitor based on self-supporting composite materials. *Journal of Power Sources 196,* 10465–10471. doi: 10.1016/j.jpowsour.2011.08.007.

Siimenson, C., Lembinen, M., Oll, O., Läll, L., Tarkanovskaja, M., Ivaništšev, V., . . . Lust, E. (2016). Electrochemical investigation of 1-ethyl-3-methylimidazolium bromide and tetrafluoroborate mixture at Bi (111) electrode interface. *Journal of The Electrochemical Society*, *163*(9), H723-H730. doi: 10.1149/2.0111609jes.

Simon, P., & Gogotsi, Y. (2010). Materials for electrochemical capacitors. *Nanoscience And Technology: A Collection of Reviews from Nature Journals*, 320-329. doi: 10.1142/ 9789814287005_0033.

Singh, S., Rakib, S., Chavhan, M., & Ganguly, S. (2016). Double layer capacitance for different thicknesses of carbon overlay and types of electrolytes: a circuit analogue approach. *Asia-Pacific Journal of Chemical Engineering*, *11*(2), 296-304. doi: 10. 1002/apj.1969.

Stoller, M., & Ruoff, R. (2010). Best practice methods for determining an electrode material's performance for ultracapacitors. *Energy & Environmental Science*, *3*(9), 1294-1301. doi: 10.1039/C0EE00074D.

Subramanian, V., Luo, C., Stephan, A. M., Nahm, K., Thomas, S., & Wei, B. (2007). Supercapacitors from activated carbon derived from banana fibers. *The Journal of Physical Chemistry C*, *111*(20), 7527-7531. doi: 10.1021/jp067009t.

Sudhan, N., Subramani, K., Karnan, M., Ilayaraja, N., & Sathish, M. (2016). Biomass-derived activated porous carbon from rice straw for a high-energy symmetric supercapacitor in aqueous and non-aqueous electrolytes. *Energy & Fuels*, *31*(1), 977-985. doi: 10.1021/acs.energyfuels.6b01829.

Sufiani, O. (2019). *Charge enhanced capacitive deionization electrodes for deionized water production* (Master's thesis) Materials Science and Engineering. The Nelson Mandela African Institution of Science and Technology.

Tokarev, K. L. (2007–2009). OpenThermo v.1.0 Beta 1 (C) ed. Retrieved from http://openthermo.software.informer.com.

Tsuzuki, S., Tokuda, H., Hayamizu, K., & Watanabe, M. (2005). Magnitude and directionality of interaction in ion pairs of ionic liquids: Relationship with ionic conductivity. *The Journal of Physical Chemistry B*, *109*(34), 16474-16481. doi: 10.1021/jp0533628.

Umebayashi, Y., Fujimori, T., Sukizaki, T., Asada, M., Fujii, K., Kanzaki, R., & Ishiguro, S. I. (2005). Evidence of conformational equilibrium of 1-ethyl-3-methylimidazolium in its ionic liquid salts: Raman spectroscopic study and quantum chemical calculations. *The Journal of Physical Chemistry A*, *109*(40), 8976-8982. doi: 10.1021/jp053476j.

Van Aken, K. L., Beidaghi, M., & Gogotsi, Y. (2015). Formulation of ionic-liquid electrolyte to expand the voltage window of supercapacitors. *Angewandte Chemie International Edition*, *54*(16), 4806-4809. doi: 10.1002/anie.201412257.

Van Aken, K. L., McDonough, J. K., Li, S., Feng, G., Chathoth, S. M., Mamontov, E., . . . Gogotsi, Y. (2014). Effect of cation on diffusion coefficient of ionic liquids at onion-like carbon electrodes. *Journal of Physics: Condensed Matter*, *26*(28), 284104. doi: 10.1088/0953-8984/26/28/284104.

Vatamanu, J., Vatamanu, M., & Bedrov, D. (2015). Non-faradaic energy storage by room temperature ionic liquids in nanoporous electrodes. *Acs Nano*, *9*(6), 5999-6017. doi: 10.1021/acsnano.5b00945.

Vu, A., Li, X., Phillips, J., Han, A., Smyrl, W. H., Bühlmann, P., & Stein, A. (2013). Three-Dimensionally Ordered Mesoporous (3DOm) Carbon Materials as Electrodes for Electrochemical Double-Layer Capacitors with Ionic Liquid Electrolytes. *Chemistry of Materials*, *25*(21), 4137-4148. doi: 10.1021/cm400915p.

Vuorilehto, K., & Nuutinen, M. (2014). Supercapacitors-Basics And Applications. *Skeleton Tech, Bautzen*. Retrieved from http://www.tgz-bautzen.de/Superkondensatoren.pdf.

Vyas, S., Dreyer, C., Slingsby, J., Bicknase, D., Porter, J. M., & Maupin, C. M. (2014). Electronic structure and spectroscopic analysis of 1-ethyl-3-methylimidazolium bis (trifluoromethylsulfonyl) imide ion pair. *The Journal of Physical Chemistry A*, *118*(34), 6873-6882. doi: 10.1021/jp5035689.

Wang, H., Wu, Y., Yuan, X., Zeng, G., Zhou, J., Wang, X., & Chew, J. W. (2018). Clay-inspired MXene-based electrochemical devices and photo-electrocatalyst: state-of-the-art progresses and challenges. *Advanced Materials*, *30*(12), 1704561. doi: 10.1002/adma.201704561.

Wang, Q., Yan, J., & Fan, Z. (2016). Carbon materials for high volumetric performance supercapacitors: design, progress, challenges and opportunities. *Energy & Environmental Science*, *9*(3), 729-762. doi: 10.1039/C5EE03109E.

Wang, Y., Song, Y., & Xia, Y. (2016). Electrochemical capacitors: mechanism, materials, systems, characterization and applications. *Chemical Society Reviews*, *45*(21), 5925-5950. doi: 10.1039/c5cs00580a.

Watanabe, M., Thomas, M. L., Zhang, S., Ueno, K., Yasuda, T., & Dokko, K. (2017). Application of ionic liquids to energy storage and conversion materials and devices. *Chemical Reviews*, *117*(10), 7190-7239. doi: 10.1021/acs.chemrev.6b00504.

Wei, D., & Ivaska, A. (2008). Applications of ionic liquids in electrochemical sensors. *Analytica Chimica Acta*, *607*(2), 126-135. doi: 10.1016/j.aca.2007.12.011.

Wei, T., Wei, X., Gao, Y., & Li, H. (2015). Large scale production of biomass-derived nitrogen-doped porous carbon materials for supercapacitors. *Electrochimica Acta*, *169*, 186-194. doi: 1016/j.electacta.2015.04.082.

Weingarth, D., Czekaj, I., Fei, Z., Foelske-Schmitz, A., Dyson, P. J., Wokaun, A., & Kötz, R. (2012). Electrochemical stability of imidazolium based ionic liquids containing cyano groups in the anion: a cyclic voltammetry, XPS and DFT study. *Journal of The Electrochemical Society*, *159*(7), H611-H615. doi: 10.1149/2.001207jes.

Weingärtner, H. (2008). Understanding ionic liquids at the molecular level: facts, problems, and controversies. *Angewandte Chemie International Edition*, *47*(4), 654-670. doi: 10.1002/anie.200604951.

Welton, T. (2018). Ionic liquids: a brief history. *Biophysics Reviews*, *10*(3), 691-706. doi: 10.1007/s12551-018-0419-2.

Wu, J., Jiang, T., Jiang, D., Jin, Z., & Henderson, D. (2011). A classical density functional theory for interfacial layering of ionic liquids. *Soft Matter*, *7*(23), 11222-11231. doi: 10.1039/C1SM06089A.

Xin, Y., & Yu, Y. X. (2017). Possibility of bare and functionalized niobium carbide MXenes for electrode materials of supercapacitors and field emitters. *Materials & Design*, *130*, 512-520. doi: 10.1016/j.matdes.2017.05.052.

Xu, W., Xiao, J., Zhang, J., Wang, D., & Zhang, J. G. (2009). Optimization of nonaqueous electrolytes for primary lithium/air batteries operated in ambient environment. *Journal of the Electrochemical Society*, *156*(10), A773-A779. doi: 10.1149/1. 3168564.

Yang, Z., Zhang, J., Kintner-Meyer, M. C., Lu, X., Choi, D., Lemmon, J. P., & Liu, J. (2011). Electrochemical energy storage for green grid. *Chemical Reviews*, *111*(5), 3577-3613. doi: 10.1021/cr100290v.

Yoo, C. G., Pu, Y., & Ragauskas, A. J. (2017). Ionic liquids: promising green solvents for lignocellulosic biomass utilization. *Current Opinion Green and Sustainable Chemistry*, *5*, 5-11. doi: 10.1016/j.cogsc.2017.03.003.

Yu, L., & Chen, G. Z. (2016). Redox electrode materials for supercapatteries. *Journal of Power Sources*, *326*, 604-612. doi: 10.1016/j.jpowsour.2016.04.095.

Yu, M., Lin, D., Feng, H., Zeng, Y., Tong, Y., & Lu, X. (2017). Boosting the energy density of carbon-based aqueous supercapacitors by optimizing the surface charge. *Angewandte Chemie International Edition*, *56*(20), 5454-5459. doi: 10.1002/ anie.201701737.

Yu, M., Lu, Y., Zheng, H., & Lu, X. (2018). New insights into the operating voltage of aqueous supercapacitors. *Chemistry–A European Journal*, *24*(15), 3639-3649. doi: 10. 1002/chem.201704420.

Zeiger, M., Jäckel, N., Mochalin, V. N., & Presser, V. (2016). Carbon onions for electrochemical energy storage. *Journal of Materials Chemistry A*, *4*(9), 3172-3196. doi: 10.1039/C5TA08295A.

Zhai, Y., Dou, Y., Zhao, D., Fulvio, P. F., Mayes, R. T., & Dai, S. (2011). Carbon materials for chemical capacitive energy storage. *Advanced Materials*, *23*(42), 4828-4850. doi: 10.1002/adma.201100984.

Zhang, L., Tsay, K., Bock, C., & Zhang, J. (2016). Ionic liquids as electrolytes for non-aqueous solutions electrochemical supercapacitors in a temperature range of 20° C–80° C. *Journal of Power Sources*, *324*, 615-624. doi: 10.1016/j.jpowsour.2016.05.008.

Zhang, L. L., & Zhao, X. (2009). Carbon-based materials as supercapacitor electrodes. *Chemical Society Reviews*, *38*(9), 2520-2531. doi: 10.1039/B813846J.

Zhurko, G. A., & Zhurko, D. A. (2015). Chemcraft Graphical Program for Visualization of Computed Results. Retrieved from http://www.chemcraftprog.com/.

APPENDICES

Appendix 1: The optimized geometrical parameters of the charged species of $[EMIM]^+$, $[BF_4]^-$, $[NTf_2]^-$ and neutral ion pair of $[EMIM][BF_4]$ and $[EMIM][NTf_2]$ in gas phase at both B3LYP5/6-311++G(d,p) and CAM-B3LYP/6-311++G(d,p) methods. The coordinates are in Appendix 1(a) - 1(e).

Appendix 1(a): Coordinates for equilibrium geometry of $[EMIM]^+$

	B3LYP5/6-311++G(d,p)			CAM-B3LYP/6-311++G(d,p)		
Atom	X, Å	Y, Å	Z, Å	X, Å	Y, Å	Z, Å
N	0.603	–2.995	–0.373	0.622	–2.996	–0.348
C	1.671	–2.246	–0.080	1.684	–2.239	–0.091
C	–0.487	–2.159	–0.521	–0.477	–2.175	–0.463
C	0.585	–4.477	–0.472	0.616	–4.469	–0.459
N	1.302	–0.961	–0.039	1.307	–0.965	–0.038
C	–0.050	–0.887	–0.314	–0.049	–0.904	–0.269
C	0.001	–5.137	0.774	–0.039	–5.130	0.741
C	2.185	0.182	0.247	2.182	0.182	0.216
H	2.668	–2.617	0.091	2.690	–2.600	0.049
H	–1.467	–2.531	–0.766	–1.461	–2.558	–0.675
H	0.012	–4.724	–1.367	0.101	–4.716	–1.387
H	1.615	–4.791	–0.645	1.655	–4.778	–0.567
H	–0.578	0.052	–0.346	–0.587	0.028	–0.282
H	0.018	–6.220	0.642	–0.014	–6.212	0.611
H	0.585	–4.894	1.664	0.488	–4.888	1.666
H	–1.035	–4.836	0.942	–1.083	–4.832	0.846
H	2.170	0.871	–0.597	2.156	0.855	–0.640
H	1.843	0.687	1.149	1.849	0.703	1.112
H	3.199	–0.183	0.397	3.199	–0.174	0.363

Appendix 1(b): Coordinates for equilibrium geometry of $[BF_4]^-$

	B3LYP5/6-311++G(d,p)			CAM-B3LYP/6-311++G(d,p)		
Atom	X, Å	Y, Å	Z, Å	X, Å	Y, Å	Z, Å
F	1.435	0.000	0.000	1.068	0.797	0.000
F	–0.478	1.353	0.000	2.203	1.433	–0.544
F	–0.478	–0.676	1.172	0.383	1.698	0.841

	B3LYP5/6-311++G(d,p)			CAM-B3LYP/6-311++G(d,p)		
Atom	X, Å	Y, Å	Z, Å	X, Å	Y, Å	Z, Å
F	–0.478	–0.676	–1.172	0.213	0.386	–1.044
B	0.000	0.000	0.000	1.473	–0.329	0.747

Appendix 1(c): Coordinates for equilibrium geometry of $[NTf_2]^-$

	B3LYP5/6-311++G(d,p)			CAM-B3LYP/6-311++G(d,p)		
Atom	X, Å	Y, Å	Z, Å	X, Å	Y, Å	Z, Å
N	8.114	–2.373	0.254	8.094	–2.108	–0.035
S	7.151	–3.284	–0.672	7.097	–3.095	–0.794
S	9.614	–1.954	–0.118	9.661	–1.972	–0.237
C	5.843	–3.573	0.663	6.134	–3.671	0.697
O	6.444	–2.540	–1.717	6.114	–2.374	–1.582
O	7.649	–4.623	–0.995	7.674	–4.309	–1.343
C	10.672	–3.233	0.796	10.380	–3.247	0.926
O	9.947	–0.711	0.574	10.102	–0.720	0.345
O	9.993	–2.120	–1.523	10.158	–2.361	–1.544
F	6.345	–4.214	1.727	6.926	–4.286	1.577
F	4.869	–4.345	0.141	5.198	–4.545	0.305
F	5.281	–2.432	1.080	5.521	–2.664	1.316
F	11.978	–2.936	0.641	11.717	–3.185	0.893
F	10.473	–4.471	0.331	10.014	–4.481	0.592
F	10.409	–3.234	2.114	9.991	–3.023	2.183

Appendix 1(d): Coordinates for equilibrium geometry of $[EMIM][BF_4]$

	B3LYP5/6-311++G(d,p)			CAM-B3LYP/6-311++G(d,p)		
Atom	X, Å	Y, Å	Z, Å	X, Å	Y, Å	Z, Å
F	–0.478	–2.158	0.171	4.953	1.642	4.693
B	0.744	–1.535	0.095	5.828	1.004	6.708
F	0.953	–0.948	–1.203	4.638	2.954	6.539
F	0.865	–0.481	1.045	6.737	2.811	5.587
F	1.820	–2.445	0.309	5.583	2.133	5.875
C	2.691	2.102	0.695	2.759	0.571	7.874
C	2.690	3.094	–0.464	1.569	1.163	8.238
N	3.716	1.046	0.536	1.215	1.157	9.254
C	3.548	–0.062	–0.191	1.901	1.421	6.082
N	4.635	–0.827	–0.059	2.934	0.746	6.569
C	5.530	–0.186	0.778	3.800	0.442	6.004
C	4.953	0.989	1.151	1.033	1.698	7.117

	B3LYP5/6-311++G(d,p)			CAM-B3LYP/6-311++G(d,p)		
Atom	X, Å	Y, Å	Z, Å	X, Å	Y, Å	Z, Å
C	4.791	–2.157	–0.664	0.124	2.253	6.971
H	2.907	2.597	1.643	1.947	3.441	4.656
H	1.736	1.584	0.794	1.927	3.769	3.616
H	2.446	2.598	–1.406	2.896	3.741	5.100
H	1.929	3.856	–0.283	1.129	3.939	5.182
H	3.657	3.594	–0.569	1.811	1.929	4.702
H	2.659	–0.317	–0.759	0.862	1.586	4.287
H	6.477	–0.621	1.045	2.628	1.463	4.155
H	5.303	1.768	1.805	3.725	–0.072	8.764
H	5.246	–2.070	–1.651	4.704	–0.020	8.289
H	5.427	–2.759	–0.016	3.434	–1.105	8.951
H	3.804	–2.615	–0.724	3.757	0.481	9.700

Appendix 1(e): Coordinates for equilibrium geometry of [EMIM][NTf_2]

	B3LYP5/6-311++G(d,p)			CAM-B3LYP/6-311++G(d,p)		
Atom	X, Å	Y, Å	Z, Å	X, Å	Y, Å	Z, Å
N	7.206	–3.773	1.063	6.345	–3.439	1.064
S	5.959	–4.777	0.975	5.761	–4.732	0.331
S	7.224	–2.220	0.664	6.583	–2.040	0.375
C	5.321	–4.784	2.754	5.329	–5.683	1.874
O	4.794	–4.294	0.204	4.467	–4.494	–0.316
O	6.423	–6.133	0.737	6.731	–5.539	–0.376
C	7.946	–2.258	–1.082	8.426	–1.989	0.112
O	8.208	–1.510	1.464	6.311	–0.953	1.297
O	5.900	–1.591	0.468	6.018	–1.933	–0.974
F	6.241	–5.240	3.599	6.394	–5.903	2.624
F	4.234	–5.571	2.832	4.809	–6.854	1.504
F	4.965	–3.544	3.127	4.415	–5.029	2.591
F	8.008	–1.006	–1.563	8.751	–0.833	–0.467
F	7.159	–2.980	–1.895	8.805	–2.986	–0.675
F	9.169	–2.782	–1.088	9.063	–2.081	1.271
N	2.009	–2.645	–0.869	1.818	–2.496	–0.638
C	3.061	–1.939	–0.435	2.999	–1.919	–0.846
C	0.969	–1.774	–1.136	0.916	–1.528	–0.257
C	1.956	–4.120	–1.002	1.533	–3.937	–0.756
N	2.722	–0.644	–0.421	2.879	–0.613	–0.616
C	1.415	–0.520	–0.857	1.580	–0.349	–0.242

	B3LYP5/6-311++G(d,p)			CAM-B3LYP/6-311++G(d,p)		
Atom	X, Å	Y, Å	Z, Å	X, Å	Y, Å	Z, Å
C	1.205	–4.774	0.153	1.275	–4.572	0.599
C	3.598	0.465	–0.013	3.961	0.375	–0.687
H	4.022	–2.347	–0.140	3.916	–2.428	–1.111
H	0.016	–2.115	–1.502	–0.112	–1.757	–0.037
H	1.480	–4.330	–1.963	0.677	–4.040	–1.424
H	2.987	–4.468	–1.034	2.405	–4.389	–1.222
H	0.926	0.435	–0.936	1.246	0.645	–0.004
H	1.189	–5.856	–0.001	1.080	–5.637	0.462
H	1.711	–4.580	1.101	2.151	–4.468	1.238
H	0.172	–4.425	0.222	0.409	–4.133	1.099
H	3.711	1.157	–0.848	3.552	1.305	–1.078
H	3.151	0.980	0.838	4.388	0.524	0.304
H	4.567	0.055	0.264	4.739	–0.006	–1.340

Appendix 2: The calculated vibrational frequencies of the charged species of $[EMIM]^+$, $[BF_4]^-$, $[NTf_2]^-$ and neutral ion pair of $[EMIM][BF_4]$ and $[EMIM][NTf_2]$ in the gas phase at both B3LYP5/6-311++G(d,p) and CAM-B3LYP/6-311++G(d,p) methods for all species. The frequencies are in Appendix 2(a) – Appendix 2(e).

Appendix 2(a): Frequencies of $[EMIM]^+$

B3LYP5/6-311++G(d,p)		CAM-B3LYP/6-311++G(d,p)	
S/N	Frequency, cm^{-1}	S/N	Frequency, cm^{-1}
1	42	1	43
2	65	2	74
3	132	3	138
4	207	4	209
5	232	5	237
6	290	6	293
7	380	7	381
8	423	8	431
9	590	9	604
10	632	10	643
11	659	11	671
12	697	12	711
13	751	13	773
14	801	14	807
15	832	15	867
16	877	16	908
17	961	17	978
18	1035	18	1052
19	1042	19	1060
20	1098	20	1110
21	1102	21	1116
22	1123	22	1133
23	1134	23	1148
24	1148	24	1159
25	1174	25	1195
26	1268	26	1281
27	1311	27	1324
28	1342	28	1374

B3LYP5/6-311++G(d,p)		CAM-B3LYP/6-311++G(d,p)	
S/N	Frequency, cm^{-1}	S/N	Frequency, cm^{-1}
29	1383	29	1398
30	1409	30	1434
31	1427	31	1442
32	1435	32	1465
33	1460	33	1473
34	1485	34	1491
35	1491	35	1498
36	1493	36	1500
37	1508	37	1516
38	1510	38	1520
39	1592	39	1629
40	1602	40	1636
41	3041	41	3069
42	3064	42	3091
43	3074	43	3103
44	3105	44	3136
45	3117	45	3149
46	3129	46	3159
47	3144	47	3176
48	3159	48	3188
49	3268	49	3288
50	3272	50	3290
51	3285	51	3306

Appendix 2(b): Frequencies of $[BF_4]^-$

B3LYP5/6-311++G(d,p)		CAM-B3LYP/6-311++G(d,p)	
S/N	Frequency, cm^{-1}	S/N	Frequency, cm^{-1}
1	337	1	338
2	337	2	339
3	498	3	503
4	498	4	503
5	498	5	504
6	732	6	753
7	1026	7	1065
8	1026	8	1066
9	1027	9	1066

Appendix 2(c): Frequencies of $[NTf_2]^-$

B3LYP5/6-311++G(d,p)		CAM-B3LYP/6-311++G(d,p)	
S/N	Frequency, cm^{-1}	S/N	Frequency, cm^{-1}
1	13	1	14
2	32	2	35
3	44	3	45
4	66	4	65
5	94	5	112
6	146	6	154
7	164	7	181
8	190	8	198
9	195	9	199
10	258	10	272
11	265	11	278
12	288	12	300
13	307	13	319
14	312	14	324
15	334	15	343
16	384	16	395
17	447	17	431
18	485	18	505
19	502	19	526
20	533	20	548
21	546	21	559
22	550	22	569

B3LYP5/6-311++G(d,p)		CAM-B3LYP/6-311++G(d,p)	
S/N	Frequency, cm^{-1}	S/N	Frequency, cm^{-1}
23	555	23	571
24	575	24	594
25	635	25	648
26	702	26	733
27	742	27	766
28	753	28	780
29	1004	29	1065
30	1077	30	1132
31	1092	31	1142
32	1141	32	1191
33	1145	33	1193
34	1156	34	1202
35	1163	35	1206
36	1183	36	1240
37	1191	37	1242
38	1268	38	1319
39	1284	39	1338

Appendix 2(d): Frequencies of [EMIM][BF_4]

B3LYP5/6-311++G(d,p)		CAM-B3LYP/6-311++G(d,p)	
S/N	Frequency, cm^{-1}	S/N	Frequency, cm^{-1}
1	8	1	26
2	26	2	49
3	47	3	68
4	51	4	77
5	88	5	93
6	95	6	105
7	110	7	109
8	123	8	132
9	168	9	182
10	211	10	229
11	237	11	244
12	302	12	306
13	344	13	346
14	345	14	350
15	392	15	391
16	423	16	442

B3LYP5/6-311++G(d,p)		CAM-B3LYP/6-311++G(d,p)	
S/N	Frequency, cm^{-1}	S/N	Frequency, cm^{-1}
17	496	17	506
18	500	18	507
19	508	19	514
20	595	20	612
21	634	21	650
22	671	22	681
23	708	23	717
24	731	24	753
25	734	25	755
26	809	26	819
27	843	27	884
28	946	28	955
29	964	29	979
30	978	30	996
31	982	31	1023
32	1040	32	1056
33	1048	33	1065
34	1106	34	1117
35	1111	35	1123
36	1119	36	1130
37	1137	37	1158
38	1155	38	1168
39	1160	39	1191
40	1195	40	1199
41	1279	41	1286
42	1322	42	1329
43	1355	43	1380
44	1396	44	1400
45	1406	45	1430
46	1423	46	1441
47	1452	47	1472
48	1461	48	1482
49	1492	49	1497
50	1499	50	1507
51	1503	51	1511
52	1508	52	1520
53	1515	53	1521

B3LYP5/6-311++G(d,p)		CAM-B3LYP/6-311++G(d,p)	
S/N	Frequency, cm^{-1}	S/N	Frequency, cm^{-1}
54	1594	54	1629
55	1600	55	1635
56	3032	56	3062
57	3054	57	3080
58	3070	58	3090
59	3095	59	3132
60	3107	60	3158
61	3127	61	3166
62	3135	62	3168
63	3148	63	3181
64	3155	64	3288
65	3270	65	3293
66	3289	66	3312

Appendix 2(e): Frequencies of [EMIM][NTf_2]

B3LYP5/6-311++G(d,p)		CAM-B3LYP/6-311++G(d,p)	
S/N	Frequency, cm^{-1}	S/N	Frequency, cm^{-1}
1	3	1	11
2	8	2	23
3	25	3	27
4	30	4	32
5	33	5	43
6	40	6	43
7	43	7	57
8	58	8	69
9	70	9	75
10	102	10	92
11	110	11	98
12	112	12	125
13	117	13	130
14	137	14	148
15	181	15	161
16	193	16	179
17	197	17	204
18	210	18	215
19	213	19	221
20	233	20	242

B3LYP5/6-311++G(d,p)		CAM-B3LYP/6-311++G(d,p)	
S/N	Frequency, cm^{-1}	S/N	Frequency, cm^{-1}
21	261	21	275
22	281	22	285
23	293	23	300
24	296	24	313
25	311	25	327
26	324	26	332
27	325	27	348
28	380	28	386
29	383	29	403
30	396	30	437
31	431	31	461
32	496	32	503
33	522	33	518
34	539	34	550
35	548	35	563
36	555	36	565
37	567	37	572
38	585	38	606
39	592	39	607
40	605	40	649
41	635	41	661
42	666	42	679
43	701	43	714
44	708	44	741
45	741	45	761
46	747	46	775
47	759	47	795
48	808	48	811
49	852	49	889
50	956	50	965
51	963	51	981
52	1006	52	1051
53	1036	53	1057
54	1041	54	1061
55	1065	55	1109
56	1074	56	1117
57	1102	57	1120

B3LYP5/6-311++G(d,p)		CAM-B3LYP/6-311++G(d,p)	
S/N	Frequency, cm^{-1}	S/N	Frequency, cm^{-1}
58	1108	58	1129
59	1118	59	1130
60	1137	60	1151
61	1149	61	1168
62	1155	62	1190
63	1160	63	1203
64	1165	64	1212
65	1178	65	1227
66	1181	66	1231
67	1192	67	1237
68	1197	68	1249
69	1266	69	1281
70	1277	70	1300
71	1291	71	1317
72	1314	72	1328
73	1344	73	1379
74	1388	74	1401
75	1410	75	1429
76	1423	76	1439
77	1447	77	1471
78	1464	78	1481
79	1490	79	1494
80	1496	80	1496
81	1503	81	1505
82	1508	82	1516
83	1512	83	1523
84	1581	84	1618
85	1603	85	1634
86	3033	86	3064
87	3051	87	3089
88	3066	88	3094
89	3099	89	3132
90	3116	90	3157
91	3127	91	3172
92	3145	92	3179
93	3154	93	3201
94	3175	94	3240

B3LYP5/6-311++G(d,p)		CAM-B3LYP/6-311++G(d,p)	
S/N	Frequency, cm^{-1}	S/N	Frequency, cm^{-1}
95	3270	95	3292
96	3289	96	3311

Appendix 3: The thermodynamic functions of the charged species of $[EMIM]^+$, $[BF_4]^-$, $[NTf_2]^-$ and neutral ion pair of $[EMIM][BF_4]$ and $[EMIM][NTf_2]$ in the gas phase and are presented in Appendix 3(a) – Appendix 3(j).

The molar heat capacity (c^o_p), entropy ($S°$) and reduced Gibbs free energy (Φ^o (T)) are given in J·mol^{-1} K^{-1}, the enthalpy increment ($H°(T)–H°(0)$) is given in kJ mol^{-1}. The thermodynamic functions were calculated using geometrical parameters and frequencies obtained by using B3LYP5/6-311++G(d,p) and CAM-B3LYP/6-311++G(d,p) methods.

Appendix 3(a): Thermodynamic functions of the $[EMIM]^+$ ion using B3LYP5/6-311++G(d,p)

T, K	$c^o_p(T)$, J mol^{-1} K^{-1}	$S°(T)$, J mol^{-1} K^{-1}	$H°(T)–H°(0)$, kJ mol^{-1}	Φ^o (T), J mol^{-1} K^{-1}
100	67.4	279.2	5.0	228.8
200	98.3	335.1	13.3	268.7
298.15	135.5	381.1	24.7	298.2
300	136.3	382	25.0	298.8
400	177.1	426.8	40.6	325.2
450	196.3	448.8	50.0	337.7
500	214.3	470.4	60.3	349.9
600	245.8	512.3	83.3	373.5
700	272.1	552.2	109.2	396.2
800	294.3	590.1	137.6	418.1
900	313.2	625.9	168.0	439.2
1000	329.5	659.7	200.1	459.6

Appendix 3(b): Thermodynamic functions of the $[EMIM]^+$ ion using CAM-B3LYP/6-311++G(d,p).

T, K	$c^o_p(T)$, J mol^{-1} K^{-1}	$S°(T)$, J mol^{-1} K^{-1}	$H°(T)–H°(0)$, kJ mol^{-1}	Φ^o (T), J mol^{-1} K^{-1}
100	66.7	277.4	5.0	227.7
200	97.1	332.8	13.1	267.1
298.15	133.5	378.1	24.4	296.3
300	134.2	379	24.6	296.8
400	174.6	423.1	40.1	322.9
450	193.8	444.8	49.3	335.2
500	211.7	466.2	59.4	347.3
600	243.3	507.6	82.2	370.6
700	269.8	547.2	107.9	393
800	292.2	584.7	136.1	414.6

T, K	$c^o_p(T)$, J mol^{-1} K^{-1}	$S°(T)$, J mol^{-1} K^{-1}	$H°(T)–H°(0)$, kJ mol^{-1}	Φº (T), J mol^{-1} K^{-1}
900	311.3	620.3	166.3	435.5
1000	327.6	653.9	198.2	455.7

Appendix 3(c): Thermodynamic functions of the $[BF_4]^-$ ions using B3LYP5/6-311++G(d,p).

T, K	$c^o_p(T)$, J mol^{-1} K^{-1}	$S°(T)$, J mol^{-1} K^{-1}	$H°(T)–H°(0)$, kJ mol^{-1}	Φº (T), J mol^{-1} K^{-1}
100	37.4	214.8	3.4	180.8
200	55.1	246.1	8.0	206
298.15	70	271	14.2	223.4
300	70.3	271.5	14.3	223.7
400	80.9	293.2	21.9	238.4
450	84.9	303	26.1	245.1
500	88.2	312.1	30.4	251.3
600	93.1	328.7	39.5	262.9
700	96.5	343.3	49.0	273.3
800	98.9	356.3	58.7	282.9
900	100.6	368.1	68.7	291.7
1000	101.9	378.7	248.4	629.4

Appendix 3(d): Thermodynamic functions of the $[BF_4]^-$ ion using CAM-B3LYP/6-311++G(d,p)

T, K	$c^o_p(T)$, J mol^{-1} K^{-1}	$S°(T)$, J mol^{-1} K^{-1}	$H°(T)–H°(0)$, kJ mol^{-1}	Φº (T), J mol^{-1} K^{-1}
100	37.3	214.4	3.4	180.4
200	54.7	245.5	8.0	205.5
298.15	69.2	270.1	14.1	222.8
300	69.4	270.6	14.2	223.1
400	80.1	292.1	21.7	237.7
450	84.1	301.7	25.8	244.3
500	87.4	310.8	30.1	250.5
600	92.4	327.2	39.1	262
700	95.9	341.7	48.6	272.3
800	98.4	354.7	58.3	281.8
900	100.2	366.4	68.2	290.6
1000	101.6	377	78.3	298.7

Appendix 3(e): Thermodynamic functions of the $[NTf_2]^-$ ion using B3LYP5/6-311++G(d,p)

T, K	$c^o_p(T)$, J mol^{-1} K^{-1}	$S°(T)$, J mol^{-1} K^{-1}	$H°(T)–H°(0)$, kJ mol^{-1}	Φº (T), J mol^{-1} K^{-1}
100	109.9	359.1	7.4	285.5
200	173	455.5	21.6	347.4
298.15	219.4	533.7	41.0	396.2
300	220.1	535.1	41.4	397
400	255	603.4	65.3	440.3
450	268.6	634.3	78.4	460.1
500	280.1	663.2	92.1	479
600	297.9	715.9	121.0	514.2
700	310.7	762.8	151.5	546.4
800	320	805	183.0	576.2
900	326.9	843.1	215.4	603.7
1000	332.1	877.8	248.4	629.4

Appendix 3(f): Thermodynamic functions of the $[NTf_2]^-$ ion using CAM-B3LYP/6-311++G(d,p)

T, K	$c^o_p(T)$, J mol^{-1} K^{-1}	$S°(T)$, J mol^{-1} K^{-1}	$H°(T)–H°(0)$, kJ mol^{-1}	Φº (T), J mol^{-1} K^{-1}
100	106.8	353.9	7.2	282.3
200	169.3	448.1	21.1	342.5
298.15	215	524.6	40.1	390.2
300	215.8	526	40.5	391
400	250.5	593	63.9	433.4
450	264.3	623.4	76.8	452.8
500	276	651.8	90.3	471.3
600	294.3	703.9	118.8	505.8
700	307.6	750.3	149.0	537.5
800	317.4	792	180.2	566.7
900	324.7	829.9	212.4	593.9
1000	330.2	864.4	245.1	619.2

Appendix 3(g): Thermodynamic functions of the [EMIM][BF_4] using B3LYP5/6-311++G(d,p)

T, K	$c^o_p(T)$, J mol^{-1} K^{-1}	$S°(T)$, J mol^{-1} K^{-1}	$H°(T)–H°(0)$, kJ mol^{-1}	Φº (T), J mol^{-1} K^{-1}
100	114.1	367.6	8.0	287.9
200	167.1	463	22.0	352.8
298.15	219.8	539.5	41.0	402
300	220.8	540.9	41.4	402.8
400	272.5	611.6	66.1	446.3
450	295.9	645.1	80.3	466.5

T, K	$c^o_p(T)$, J mol^{-1} K^{-1}	$S°(T)$, J mol^{-1} K^{-1}	$H°(T)–H°(0)$, kJ mol^{-1}	Φº (T), J mol^{-1} K^{-1}
500	317.2	677.4	95.7	486
600	353.9	738.6	129.3	523.1
700	384	795.5	166.2	558
800	408.9	848.4	205.9	591
900	429.7	897.8	247.9	622.4
1000	447.4	944	291.8	652.3

Appendix 3(h): Thermodynamic functions of the [EMIM][BF_4] using CAM-B3LYP/6-311++G(d,p)

T, K	$c^o_p(T)$, J mol^{-1} K^{-1}	$S°(T)$, J mol^{-1} K^{-1}	$H°(T)–H°(0)$, kJ mol^{-1}	Φº (T), J mol^{-1} K^{-1}
100	111	342.6	7.4	268.5
200	164.4	436.2	21.2	330.1
298.15	216.7	511.6	39.9	377.7
300	217.7	512.9	40.3	378.5
400	269.2	582.7	64.7	421
450	292.6	615.8	78.8	440.8
500	314	647.7	93.9	459.9
600	351	708.4	127.2	496.3
700	381.2	764.8	163.9	530.7
800	406.3	817.4	203.3	563.3
900	427.3	866.5	245.0	594.3
1000	445.2	912.5	288.7	623.8

Appendix 3(i): Thermodynamic functions of the [EMIM][NTf_2] using B3LYP5/6-311++G(d,p)

T, K	$c^o_p(T)$, J mol^{-1} K^{-1}	$S°(T)$, J mol^{-1} K^{-1}	$H°(T)–H°(0)$, kJ mol^{-1}	Φº (T), J mol^{-1} K^{-1}
100	185.5	486.7	12.1	366.2
200	284.6	646.9	35.7	468.2
298.15	369.1	776.6	67.9	548.9
300	370.6	778.8	68.6	550.3
400	446.7	896.2	109.5	622.3
450	479.7	950.7	132.7	655.8
500	509.3	1002.8	157.4	687.9
600	559	1100.3	211.0	748.7
700	598.4	1189.5	268.9	805.4
800	630.1	1271.5	330.4	858.6
900	656.1	1347.3	394.7	908.7
1000	677.7	1417.6	461.5	956.1

Appendix 3(j): Thermodynamic functions of the [EMIM][NTf_2] using CAM-B3LYP/6-311++G(d,p)

T, K	$c^o_p(T)$, J mol^{-1} K^{-1}	$S°(T)$, J mol^{-1} K^{-1}	$H°(T)–H°(0)$, kJ mol^{-1}	Φº (T), J mol^{-1} K^{-1}
100	182.2	459.4	11.6	342.9
200	279	616.5	34.9	442.1
298.15	362.3	743.6	66.4	520.9
300	363.8	745.9	67.1	522.3
400	439.6	861.2	107.3	592.9
450	472.8	914.9	130.2	625.7
500	502.6	966.3	154.6	657.2
600	553	1062.6	207.4	716.9
700	593.1	1151	264.8	772.6
800	625.4	1232.3	325.8	825.1
900	651.9	1307.6	389.7	874.6
1000	673.9	1377.4	456.0	921.4